Manuscript prepared for Glob. Change Biol.

Date: 7 April 2017

Big in the benthos: Future change of seafloor community biomass in a global, body size-resolved model

Andrew Yool[1], **Adrian P. Martin**[1], **Thomas R. Anderson**[1], **Brian J. Bett**[1], **Daniel O.B. Jones**[1], **and Henry A. Ruhl**[1]

[1]National Oceanography Centre, University of Southampton Waterfront Campus, European Way, Southampton SO14 3ZH, UK

Correspondence to: A. Yool (axy@noc.ac.uk)

Running title: Big in the benthos

Keywords: benthic, global, model, allometric, seafloor, future, ecology, POC flux

Abstract

Deep-water benthic communities in the ocean are almost wholly dependent on near-surface pelagic ecosystems for their supply of energy and material resources. Primary production in sunlit surface waters is channelled through complex food webs that extensively recycle organic material, but lose a fraction as particulate organic carbon (POC) that sinks into the ocean interior. This exported production is further rarefied by microbial breakdown in the abyssal ocean, but a residual ultimately drives diverse assemblages of seafloor heterotrophs. Advances have led to an understanding of the importance of size (body mass) in structuring these communities. Here we force a size-resolved benthic biomass model, BORIS, using seafloor POC flux from a coupled ocean-biogeochemistry model, NEMO-MEDUSA, to investigate global patterns in benthic biomass. BORIS resolves 16 size-classes of metazoans, successively doubling in mass from approximately 1μg to 28mg. Simulations find a wide range of seasonal responses to differing patterns of POC forcing, with both a decline in seasonal variability, and an increase in peak lag times with increasing body size. However, the dominant factor for modelled benthic communities is the integrated magnitude of POC reaching the seafloor rather than its seasonal pattern. Scenarios of POC forcing under climate change and ocean acidification are then applied to investigate how benthic communities may change under different future conditions. Against a backdrop of falling surface primary production (-6.1%), and driven by changes in pelagic remineralisation with depth, results show that while benthic communities in shallow seas generally show higher biomass in a warmed world (+3.2%), deep-sea communities experience a substantial decline (-32%) under a high greenhouse gas emissions scenario. Our results underscore the importance for benthic ecology of reducing uncertainty in the magnitude and seasonality of seafloor POC fluxes, as well as the importance of studying a broader range of seafloor environments for future model development.

1 Introduction

Of the particulate organic carbon (POC) fixed annually in the surface ocean by primary producers ($\approx$ 45 Pg C y^{-1}; Behrenfeld and Falkowski, 1997), almost all is remineralised back to dissolved inorganic carbon (DIC) within a short time period (months to years). However, mediated by a complex community of benthic organisms, a small fraction of this POC (0.05 Pg C y^{-1}; Hain et al., 2014) is sequestered by seafloor burial, and represents a significant flux on geological time scales (Mawbey and Lear, 2013). This same community also remineralises POC, turning it back to DIC and nutrients that eventually resupply productive surface communities (Dunne et al., 2007). Consequently, understanding the role that benthic communities play in the biogeochemical cycles of the ocean, and estimating how this role may change into the future, is of considerable interest (e.g. Moodley et al., 2011; Kriest and Oschlies, 2013).

Benthic communities are an important source of commercially exploited seafood, both for direct human consumption, and for other harvested species. They are also often highly biodiverse, and in the deep sea may be relatively pristine compared to other marine habitats more directly impacted by human activities (Ramirez-Llodra et al., 2011; Jackson et al., 2001; Lotze et al., 2006). As such, they may be indicators of anthropogenic change in deep-sea habitats (Rees et al., 2006), whether that be by global-scale climate change or ocean acidification (Yasuhara et al., 2008; Mora et al., 2013; Birchenough et al., 2015; Sweetman et al., 2017), or by local seafloor mineral extraction (Halfar and Fujita, 2007).

Advances in deep-sea photography (e.g. Bett, 2003), sampling (e.g. Gooday et al., 1998) and even *in situ* experimentation (e.g. Witte et al., 2003; Nomaki et al., 2005; Jeffreys et al., 2013; Main et al., 2015) have significantly increased understanding of how these communities are organised (Danovaro et al., 2014). Evidence suggests that food web complexity and functional groupings of organisms may be of secondary importance to body size in controlling energy flow through these communities (Peters, 1983; Dickie et al., 1987; Brown et al., 2004; Blanchard et al., 2017). As body mass is readily quantified, and well-correlated with metabolic processes (e.g. Brey, 2010) as well as community biomass and abundance (e.g. Hildrew et al., 2007), this is attractive on both practical and theoretical grounds. However, there is still considerable debate among biologists and ecologists as to the causes, and universality, of the mass-scaling of metabolism (e.g. Glazier, 2005; Hunt and Roy, 2006; Hildrew et al., 2007; Glazier, 2010). Nevertheless, the continuing development of the Metabolic Theory of Ecology (McClain et al., 2012; Schramski et al., 2015) demonstrates the practical value of size-based assessments of ecosystem function. Allometry has proven a useful concept in both terrestrial and aquatic ecology (e.g. Schmidt-Nielsen, 1984, Hildrew et al., 2007), and its application to benthic communities, and marine systems in general, has clear potential (e.g. Blanchard et al., 2009; Blanchard et al., 2017).

As a preliminary step towards this, Kelly-Gerreyn et al. (2014) introduced an allometry-based model of the seafloor metazoan community that reproduced the distribution of biomass and abundance at three contrasting locations: (i) Faroe-Shetland Channel, North Atlantic deep sea, (ii) Fladen Ground, North Sea continental shelf, and (iii) Oman Margin, Arabian Sea continental slope (see Section 2.1.1 for more details). They employed high quality size-resolved observational data on the meio- and

macrobenthos from these three sites. Their model was tuned for these locations individually, and subsequently retuned to all three sites simultaneously to provide a more broadly applicable, or "unified" parameterisation (Ichino et al., 2015; see Section 2.1.1 and Appendix A2). The three study locations are highly contrasting in terms of water depth, habitat temperature, and the magnitude and seasonality of productivity. Consequently, Kelly-Gerreyn et al. (2014) consequently suggested that the model was likely to be robust and of broad application to marine benthic communities.

Future forecast simulations indicate that primary production – the key driver of the Kelly-Gerreyn et al. (2014) model – may be seriously impacted by climate change during the 21st century. The Coupled Model Intercomparison Project (CMIP5) used in Assessment Report 5 (AR5) of the Intergovernmental Panel on Climate Change (IPCC) found that, under a high greenhouse gas emissions scenario (RCP 8.5; see Section 2.2.1), primary production changed by an average of -8.1%, with falls in export production being even greater, ranging from -7% to -16% (Bopp et al., 2013). Similar results were found by Yool et al. (2013b), who inferred a link with ocean acidification (OA), which led to drops in primary production (-6.3%) translating to much larger declines in export flux to the deep ocean (-40.7% at 1000 m water depth). Using simulated changes in export flux and an empirical seafloor biomass model, Jones et al. (2014) estimated that an average change in seafloor POC flux of -11.4% translated to a decline in total benthic biomass of -5.2% at the global scale. These changes suggest that benthic communities will experience substantial impact in the near future.

In addition to changes in the food supply available to them, although not examined here, it is anticipated that benthic communities will experience other stresses. Temperature has been already been identified as a key stressor from palaeological records (Yasuhara et al., 2014), especially where it is naturally low or high and organisms are most vulnerable to change (Yasuhara and Danovaro, 2016). More broadly, much as with pelagic communities (Gruber, 2011; Popova et al., 2016), benthic communities are also vulnerable to additional anthropogenically-driven stressors, including acidification, deoxygenation and contamination (Levin and Le Bris, 2015). Exposure to stressors such as temperature and acidification would likely be strongly depth-dependent because of their surface sources, but the other stressors may be communicated more directly to the deep ocean through the biological pump (deoxygenation) or gravitational sinking (contamination).

Here we take the Kelly-Gerreyn et al. (2014)'s allometry-based model of the benthic community and force it with POC fluxes derived from the pelagic ecosystem model of Yool et al. (2013b). The model's unperturbed behaviour is examined, both in terms of global geographical variability and the role of temporal variability (especially seasonality) in POC flux. How these features may change into the future is then investigated using two end-member IPCC AR5 scenarios for the 21st century (RCPs 2.6 and 8.5). We focus on the outcomes for integrated seafloor biomass and its distribution across the modelled size classes, and how both of these properties vary in space and time.

2 Materials and Methods

2.1 BORIS model

The benthic community is modelled using the Benthic Organisms Resolved In Size v1.0 (BORIS-1; henceforth BORIS) model (Kelly-Gerreyn et al., 2014)[1], which represents the biomasses of seafloor metazoans in the meio- to macrofaunal size range (0.9 μg wet wt to 30 mg wet wt; see Table S1). This size range was selected based on the availability of high quality size-resolved field data. POC flux consumption and subsequent respiration by smaller and larger organisms are represented implicitly via the f_{other} parameter (see Appendix A1). As illustrated in Figure 1a, the model is driven by the POC flux reaching the seafloor which, after a fixed fraction is consumed by the implicit respiration of other members of the benthos, enters a detrital reservoir that is accessed by the modelled metazoans, both as a source of food (ingestion) and a sink for losses (mortality, defecation). Ultimately, all of the POC that arrives at the seafloor is consumed and respired, i.e. burial sequestration is assumed to be minimal, and the model provides a biomass size-distribution of the modelled metazoan community. Long-term observations of POC flux to the seabed and corresponding sediment community respiration in the deep ocean suggest that this is a reasonable simplification (Smith and Kaufmann, 1999; Smith et al., 2009). Similarly, global scale assessments of the deep-ocean (> 2000 m water depth) POC burial flux suggest a value of only 3% of seafloor POC flux (Dunne et al., 2007).

Appendix A1 presents a detailed description of the structure, parameterisation and evaluation of BORIS. The computational implementation of BORIS is described in Appendix A3.

2.1.1 Default performance

In Kelly-Gerreyn et al. (2014), the 8 model parameters in BORIS were tuned using a micro-genetic algorithm approach (Ward et al., 2010). This was done separately for each of the three field locations. The procedure is fully described in Kelly-Gerreyn et al. (2014), and summarised in Appendix A2.

The field data used to calibrate BORIS came from: Faroe-Shetland Channel (FSC; 61.92°N, 2.80°W; 1623m water depth), Fladen Ground (FG; 58.27°N, 0.88°E; 153m), and Oman Margin (OM; 23.38°N, 59.00°E; 507m). Figure 1b shows these locations. Table S2 lists the values of the parameters derived by Kelly-Gerreyn et al. (2014) for the three sites, together with the ranges from which they were drawn. Also listed is a "unified" parameter set (column **All**) that was produced using the same approach as in Kelly-Gerreyn et al. (2014), but fitting the model to all three sites simultaneously. This parameter set was previously employed by Ichino et al. (2015), and is used throughout the present study.

Figure S1a shows the resulting biomass distributions across the modelled size classes at equilibrium for the three locations. The model reproduces the observed general rise in standing stock with body size. The performance of the model tuned for individual locations (r^2 = 0.96, 0.67, 0.07) is better than that of the unified model (r^2 = 0.76, 0.41, 0.04).

[1]In Kelly-Gerreyn et al. (2014), the model was not explicitly given a name, but we adopt the moniker BORIS here to facilitate reference and discussion.

2.2 NEMO-MEDUSA

Simulations of a coupled ocean-biogeochemistry model, NEMO-MEDUSA, provide the geographical and seasonal flux of POC to the seafloor. The physical ocean component is the Nucleus for European Modelling of the Ocean (NEMO) (Madec, 2008), run at 1° horizontal resolution for the global domain. The biogeochemical component is the Model of Ecosystem Dynamics, nutrient Utilisation, Sequestration and Acidification (MEDUSA; Yool et al., 2013). POC flux to the seafloor comprises two separate size classes of detrital particles, the balance of which means that shallow regions are typically dominated by "small", slow-sinking particles, while deep regions are dominated by "large", fast-sinking particles. NEMO-MEDUSA agrees well with observed deep-sea POC fluxes (Honjo et al., 2008; Yool et al., 2013). Note that POC in NEMO-MEDUSA is in molar units, while POC in BORIS is instead in wet weight units, and that these are converted using linear factors for carbon mass, dry weight and water content (Brey et al., 2010).

Appendix B1 presents more details concerning the structure, parameterisation and validation of NEMO-MEDUSA.

2.2.1 Forcing scenarios

We use extant, multi-centennial simulations of NEMO-MEDUSA as a source of seafloor POC flux for both (a) an unperturbed, control state, and (b) an anthropogenically-forced, historical state (1860–2005). The latter was extended into the future (2006–2099) under two contrasting scenarios of 21st century climate change, RCP 2.6 and RCP 8.5 (Rogelj et al., 2012). These simulations were forced at the ocean surface using output from the UK Meteorological Office's (UKMO) HadGEM2-ES Earth system model (Jones et al., 2011). The control simulation used a repeated 30-year cycle of forcing from the unperturbed portion of the historical simulation, with constant, pre-industrial pCO_2 concentrations.

In terms of POC fluxes to the seafloor, Yool et al. (2013b) found that these declined into the future in parallel with the decline in primary production driven by increasing ocean stratification and decreasing nutrient availability. However, while the decline in global primary production is modest (-6%), the corresponding decline in POC flux to the deep ocean is greater (-40%; 1000 m water depth), as a result of the role of ocean acidification. Driven by oceanic uptake of anthropogenic CO_2, this both shoals the modelled calcite compensation depth and decreases NEMO-MEDUSA's production of biogenic calcium carbonate, with the latter the dominant factor for POC fluxes.

Appendix B2 presents more details concerning these scenarios and the forcing output.

2.3 Simulations

Monthly average POC flux (g C m^{-2} d^{-1}) to the seafloor was extracted from NEMO-MEDUSA for both the control and the historical portion of the RCP simulations described above (1980–1999). A monthly climatology was produced using the output from the control simulation, i.e. consisting of average January, average February, etc. This climatology was used to force simulations of BORIS in order to explore its seasonal behaviour, initially at the three calibration sites.

These simulations were started from analytically-derived initial conditions (see Appendix A4), and then spun-up for a period of 100 years to ensure that BORIS's constituent tracers exhibited a stable seasonal cycle.

This control climatological forcing was then applied at the global scale to explore large-scale geographical patterns in the behaviour of BORIS for unperturbed conditions. Simulations of 100-year duration were performed separately at each location in the NEMO-MEDUSA grid (65238 cells in total; 62% of the 360×292 domain), and analysis made use of the average seasonal cycle in the final decade of the simulation. Each grid location was assumed to be independent of adjacent locations and dependent solely on POC falling from above.

This analysis was then extended using historical (1980–2005) and future (2006–2099) forcing to investigate the response of the modelled benthic ecosystem to changes in the POC flux driven by climate change and ocean acidification. In this case, BORIS was initialised at each geographical location from the corresponding end-state of the climatological control simulation, and then run for the period 1980–2099, with parallel RCP 2.6 and RCP 8.5 scenarios for the 2006–2099 period. Unlike the situation with climatological forcing, because of the time-varying nature of the forcing in these latter cases, analysis of the results used output from the full period rather than only the end of the simulation.

In all simulations of BORIS, the seafloor POC fluxes provided by NEMO-MEDUSA were first amended by subtracting a fixed and geographically uniform proportion of POC – the parameter f_{other}. As noted above, this is designed to account for the fraction consumed by unmodelled seafloor organisms (e.g. microbes and megabenthos). The remaining POC entered the seafloor detritus pool at which point it became available for BORIS's modelled metazoan size classes. This parameterisation is discussed further later, and details concerning it can be found in Appendix A1. As noted earlier, organisms outside the size range considered by BORIS (larger and smaller) consume a portion of the POC flux, and the feeding relationship of all of these organisms on seafloor POC is much more complex than the simple transfer to respiration represented here.

3 Results

In the following, BORIS only implicitly represents both smaller and larger size classes that contribute to complete seafloor biomass. Consequently, the term "total biomass" is used in the presentation of results from BORIS to refer specifically to the total biomass of the modelled size classes resolved by BORIS and not to the complete total seafloor biomass of living organisms.

3.1 Site simulations

Table 1 presents the observed and modelled seafloor POC fluxes for the three sites alongside both those observed, and those from the optimised BORIS model (per Table S2). The input POC flux that is available to the modelled size classes of BORIS, Q, is a fraction of the total flux reaching the seafloor, and the observed fluxes in Table 1 are accompanied by inferred values of parameter f_{other} that determine the fraction of the seafloor POC flux that is consumed by unmodelled size classes. In the case of all three sites, f_{other} is greater than 0.9 and, in the case of FG, exceeds 0.98, i.e. less than 2% of the seafloor POC flux is available to the modelled benthic metazoans. This partitioning of food consumption is consistent with studies such as those of Pfannkuche and Soltwedel (1998) which found continental slope benthic systems to be dominated by bacteria and other small size class biomass (> 90%). Similarly, in situ deep-sea measurements (e.g. Witte et al., 2003) have suggested that since microbes account for 95% of benthic biomass, they likely dominate total seafloor community respiration.

In a similar fashion, Table 1 also reports the seafloor POC fluxes of NEMO-MEDUSA accompanied by inferred values of f_{other} for both control and historical periods. While these model-inferred values agree well with the observation-inferred values for the FG site, i.e. are consistently close to 0.98, those for the other two sites are lower – in the case of the FSC site, inferred f_{other} values are only around 0.3. As Appendix C describes, this discrepancy remains even where a larger 3×3 area around the sites is considered to account for grid mismatches, though the low value of f_{other} inferred at FSC (0.34) is consistent with a low productivity bias in the subpolar North Atlantic in NEMO-MEDUSA, noted by Yool et al. (2013).

The NEMO-MEDUSA values of seafloor POC flux reported in Table 1 are multi-decadal averages, but the model, as well as reality, exhibits significant temporal variability. Variability occurs at all three stations, ranging from seasonal, through inter-annual to decadal-scale patterns (Section 3.3), as illustrated in Figure S2, and considered further in Appendix C.

Taking the seasonal climatology of seafloor POC fluxes at the three geographical sites from the control simulation (Figure S2), and applying them to BORIS at the three sites using a uniform value of f_{other} of 0.9 (Appendix C), Figure S1b shows the resulting seasonal patterns of biomass for the modelled size classes and the seafloor detrital pool, R. Seabed flux at the three sites exhibits strong seasonal variability, and BORIS responds to this variability differently between the three sites. This is seen in Table S3 by the variable lags to POC flux shown by different benthic components. Total biomass is found to lag POC flux least at FG (52 days), is intermediate at FSC (90 days), but lags by 200 days at OM. While this suggests an interesting

complexity in the relationship between POC flux and benthic communities, the three calibration sites alone cannot address this detail.

3.2 Global patterns

Although the three calibration sites examined above vary in both total POC flux and in seasonal pattern, they represent only a fraction of the global range in these properties. Figure 2 shows the annual mean and coefficient of variation (CoV) of the climatological POC flux of NEMO-MEDUSA. This flux is primarily a function of export production (itself related to local primary production) and seafloor depth, with the highest values in the productive shallow waters of coastal regions, and the lowest values in the oligotrophic deep-water areas of the open ocean. Water depth plays a critical role in setting the seafloor flux, since it effectively sets the timescale over which POC sinking through a water column experiences remineralisation. In shallow water regions, this is typically a short period of time, so much of the POC exported reaches the seafloor, while in deep-water regions, sinking and remineralisation periods are extended and seafloor POC fluxes are a much smaller fraction of export (see also Appendix B1). Across the global ocean, NEMO-MEDUSA simulates a range in seafloor POC flux that spans 12 orders of magnitude (Figure 3b). Patterns in seasonality are somewhat more complicated, with CoV values that are independent of both productivity and water column depth. With the exception of the high latitude Antarctic and Arctic, where POC fluxes are understandably strongly seasonal, there are no discernible zonal patterns comparable to those in the seafloor POC flux itself. Areas of similar productivity can exhibit quite different seasonality, based on prevailing hydrography, such as major currents, or on features in surface forcing driven by local weather patterns.

Figure 3a and Figure S3 show the resulting patterns of annual mean seafloor detritus and total biomass (the sum of all explicitly modelled biomass classes) when forced by these POC fluxes. As expected, the relationships between POC flux and seafloor detritus or biomass are very close (Figure 2a), with the same patterns of lows in the oligotrophic gyres and highs in productive shelf regions. To illustrate the strength and consistency of these relationships, Figure 3b plots annual mean seafloor detritus and biomass for each size class against annual mean POC flux. Clearly, the patterns are exceptionally strong, with nearly perfectly linear (in a log-log sense) relationships between seafloor POC flux and all of the components of BORIS. There is a low level of spread around the general correspondence. This variability is potentially caused by differences in seasonal patterns of POC flux, but this is very modest by comparison to the mean annual response. For comparison, Figure S4d illustrates the influence of seasonality in these patterns by repeating Figure 3b with monthly data. This illustrates that while BORIS is well-constrained by POC flux on a mean annual basis, its seasonal behaviour can be considerably more complex.

Seasonality and temporal lags in the global model are examined in Figure S5. The majority of model grid cells lie towards higher POC fluxes though are well spread on the CoV (seasonality) axis.

Projected across this POC flux domain, Figures S5b and S5c show the average time delay between annual maximum POC flux and the corresponding annual maxima in seafloor detritus and total biomass. The general pattern in average temporal lags between peak annual seafloor POC flux and seafloor detritus (Figure S5b) or modelled total biomass (Figure S5c) is for the

lag to increase with decreasing POC flux, with a tendency for shorter lags where CoV is higher (more seasonal). Figure S6 presents the corresponding lags for size classes 1 and 16, and illustrates a broadly consistent pattern of greater lags in the larger size classes (see also Figure S7).

3.3 Future change

To investigate the impact of changes in seafloor POC flux for benthic communities, Figure 4, Figure S8 and Table 2 detail the change in globally integrated seafloor biomass across the 21st century for the RCP 2.6 and RCP 8.5 scenarios described earlier (Rogelj et al., 2012).

Table 2 reports globally integrated primary production, its translation to export production and the flux of POC to the seafloor, and the resulting modelled total biomass at a series of water depth intervals from shallow seas (to 0.1km) to the full depth of the ocean (to 10km). In terms of primary production, while the extreme RCP 8.5 scenario experiences a 6.1% decline by the 2090s, control of emissions in RCP 2.6 results in a small increase in global productivity by the end of the century (in part related to slightly elevated temperatures enhancing phytoplankton growth rates). Export production shows a small decline of -1.3% under RCP 2.6 (in part related to slightly elevated temperatures enhancing remineralisation rates), but a much larger decline of -11.4% under RCP 8.5's more extreme change. Integrated to the global scale, POC fluxes to the seafloor are increased for RCP 2.6 (+8.5%), while under RCP 8.5 there is a decline (-3.9%). This seeming disparity with export production stems from the seafloor POC flux being biased towards shallow regions (where a greater fraction of export survives to the seafloor), and the exclusion of regions with depths < 100 m from the reported export production.

To separate the impact of changes in seafloor POC flux and water depth, Table 2 divides the seafloor into seven water depth bands. For the shallow seas (< 100 m water depth), both scenarios result in an increase in seafloor biomass, largely driven by warmer conditions that increase growth rates in shallow regions (Yool et al., 2013b). For both scenarios, this increase declines and then reverses (by 200 m water depth under RCP 8.5) with increasing water depth. By 5000 m water depth, seafloor biomass is lower for RCP 2.6 (-7.0%) and much lower for RCP 8.5 (-32.0%). Integrating globally, the total modelled seafloor biomass in BORIS declines slightly under RCP 2.6 (-1.1%), contrary to the corresponding increases in both primary production and seafloor POC flux. Under RCP 8.5, seafloor biomass decreases substantially (-17.6%), far more than either primary production or seafloor POC flux.

To distinguish the influences of changing primary productivity and water depth, Table 3 separates seafloor POC flux and the resulting modelled seafloor total biomass into depth bands. The pattern of increased seafloor POC flux in shallow seas and decreasing flux with increasing water depth is clear. Changes in seafloor POC flux at all water depths are greater than the corresponding changes in modelled total biomass. While the shallowest 5% of the ocean's seafloor experiences increased POC flux (+10.2%) and seafloor biomass (+3.2%), more than 83% of the ocean seafloor is at water depths greater than 2 km depth, where there are large decreases in POC flux (-53.4% or greater) and modelled total biomass (-32.0% or greater). The relationship between change in seafloor POC flux and change in modelled total biomass is strongly linear with a slope of

approximately 0.6, i.e. biomass changes less than the POC flux. This contrasts with the pelagic situation of NEMO-MEDUSA where a decline of primary production of -6.1% was much more closely paralleled by a corresponding decline of -5.7% in the biomass of surface phytoplankton (Yool et al., 2013b).

Table 2 and Figure S9 indicate how changes in primary production, export production, seafloor POC flux and seafloor biomass are correlated. In the case of export and primary production (Figure S9a), this is almost linear, with a slight bias towards decreased export, i.e. a -10% decline in primary production leads to a large decline in export, while a 10% increase in primary production leads to a slightly smaller increase in export. Similar, but less well-correlated and much less linear, relationships are apparent between seafloor POC flux and both export (Figure S9b) and primary (Figure S9d) production. However, the correlation between seafloor biomass and POC flux is strongly linear, with the variability introduced by seasonality practically insignificant when viewed across the global range.

Figure 4a and Figure S8a show corresponding plots of temporal change in globally-integrated modelled seafloor total biomass for the two scenarios. Both show relatively small changes in total biomass in shallow seas ($<$ 200 m water depth), with larger changes generally occurring at greater water depths. In the case of RCP 2.6, these changes have generally saturated – or have even reversed direction – by the middle of the 21st century, in keeping with the strong mitigation characteristic of this scenario. In marked contrast, RCP 8.5 shows strong declines in seafloor total biomass that continue throughout the century, particular at greater water depths, also in keeping with the business-as-usual nature of this scenario.

To place these changes in a geographical context, Figure 4b and Figure S8b show patterns of absolute change in biomass at the global scale. Under RCP 8.5, seafloor biomass declines across the globe, with exceptions in some shallow seas, and where the boundaries of oligotrophic gyre areas have shifted. RCP 2.6 repeats much of this pattern, but with large areas of increased seafloor total biomass, principally in the Pacific and Indian basins, where they occur in both shallow and deep-water regions. Seafloor total biomass in the Atlantic Ocean – noted for its productivity decline in Yool et al. (2013b) – broadly declines regardless of the scenario. The large shallow-water continental shelves of the Arctic Ocean show a marked increase in seafloor biomass in line with that of primary production (cf. Yool et al., 2013b; Yool et al., 2015).

4 Discussion

We have explored the spatial (global scale) and temporal (seasonal to inter-annual) response of a body mass size-resolved model of seafloor metazoan biomass, BORIS (Figure 1a), to variability in the seafloor POC fluxes that drive it.

Building on the constant seafloor POC flux forcing in Kelly-Gerreyn et al. (2014) using the NEMO-MEDUSA model's seasonally-resolved forcing, we find diversity in the seasonal response to sedimenting POC, with some regions responding rapidly to inputs of POC, while others respond more slowly (Figure S1b). Our three calibration sites represent a limited diversity in POC flux, and we extended our analysis globally giving a much broader range of POC forcing, in terms of both magnitude (Figure 2a) and seasonality (Figure 2b). This revealed further diversity in the phenological responses of BORIS (Figures 3a, S3 and S5) as well as strong, conservative patterns of biomass tied to POC supply to the seafloor (Figure 3b).

Earlier studies have noted that anthropogenic change may influence ocean productivity and thereby standing stocks of the benthos (e.g. Mora et al., 2013; Jones et al., 2014). Here we have examined the impact on seafloor biomass under end-member low (RCP 2.6) and high (RCP 8.5) IPCC emissions scenarios. While the impact on seafloor biomass was greater in the higher emissions case, both scenarios showed a similar pattern of change in which shallow seas increased in biomass while there was an increasingly negative impact with increasing water depth (Figure 4). As a result of ocean acidification-mediated change in surface-ocean communities, the high scenario used here is particularly severe for seafloor communities, and translates relatively modest change in primary productivity into substantial decreases in seafloor POC fluxes (Figures 4a and 4b; Tables 2 and 3).

The strongly seasonal response of BORIS to the model-derived POC forcing used here has potentially important implications for both observational and modelling studies.

For observational studies, the model results underscore the importance of understanding POC flux variability (seasonality) as this may drive biomass cycles. However, the difficulty of obtaining high quality body mass distribution time-series from benthic ecosystems currently severely limits the number of datasets available to further development of BORIS. As such, when direct measurements of seafloor POC flux at any location are infrequent, it is important that seasonality is investigated by examination of the surface ocean system that drives it. For instance, through the use of surface samples of nutrients and plankton or production measurements, or estimated via remote-sensing (e.g. Henson et al., 2012).

For modelling, our results suggest that the use of observational data in models needs to be based on an appropriate consideration of their temporal context. In particular, does the observation represent a stable body mass distribution or simply a single time-slice of a dynamic cycle. Model validation – and, especially, tuning – needs to ensure that model output and observational data are compared in a like-for-like manner.

While BORIS does exhibit substantial variability in response to temporally-varying POC forcing, it is also conservative with respect to the average magnitude of that forcing. Despite the wide variety in seasonal patterns of POC forcing from NEMO-MEDUSA, average seafloor detritus and total biomass in BORIS is predictable from local annual POC flux. This suggests that, when characterising seafloor dynamics, an accurate annual estimate of seafloor POC flux is critical.

It is notable that the magnitude of seasonal variability varies strongly between the model components. Seasonality is greatest for the detrital pool that the model benthos feeds on, and declines with individual body mass in the modelled size classes, such that larger organisms have noticeably lower CoV than smaller organisms (Figure S10), presumably a function of their longer life-spans and slower physiological rates (McClain et al., 2012). This has interesting implications for field sampling programmes. For instance, in areas with highly seasonal productivity and resultant seafloor POC fluxes, while the temporal nature of these fluxes needs to be well-characterised in order that the total annual flux is constrained, this may be less pressing for the benthic communities, and particularly the largest members of those communities. The largest benthic organisms (megabenthos) have until recently been difficult to quantify, however, new techniques have dramatically enhanced current capability (Morris et al., 2016). If the model's behaviour well-describes that of real communities, lower frequency sampling of the larger body mass components of the community may be sufficient to capture a representative picture in an efficient manner. This is significant given the technical difficulty and expense of sampling the seafloor.

Temporal variability can also be considered in terms of the approach to equilibrium of body mass distribution. Through idealised perturbations of the seafloor detritus pool (half and double), Figure S11 shows that the time to equilibrium for BORIS increases with decreasing seafloor POC flux, i.e. communities with lower total biomass take longer to return to equilibrium, and that it may take a very long time ($\approx$ 1 My for the lowest POC fluxes). While this extreme value is no doubt highly questionable, times ranging from years to decades of recovery have been suggested in field observations of the deep sea (e.g. Huvenne et al., 2016). This has obvious implications for appropriate environmental assessment and monitoring procedures, since recovery periods may be inversely related to total seafloor biomass. Though open-ocean benthic systems have broadly – so far – escaped major perturbations on the scales that pelagic and terrestrial ecosystems have experienced to date, the changes that may accompany global warming, ocean acidification, and increasing human exploitation of the deep-sea floor are pervasive (Halfar and Fujita, 2007; Huvenne et al., 2016).

As seafloor POC fluxes vary in time, seafloor communities do not have a fixed equilibrium to converge to, and will instead track a "moving target". Figure S12 shows dynamically-simulated and equilibrium total biomass at the three calibration sites, averaged on both monthly and annual timescales. On short timescales, the dynamic simulations struggle to follow the detailed steady states calculated analytically, though to varying degrees that correlate with POC flux magnitude, i.e. site FG has highest flux and most closely tracks the analytical steady state. However, averaged over annual timescales, the dynamic simulations relatively closely track the equilibrium states.

Figure S13 presents a global-scale examination of the relationship between dynamic simulations and equilibrium states. In general, the dynamic state is out of equilibrium to a slightly positive degree, both for the 1990s and the 2090s. The oligotrophic gyres are regions of larger disequilibrium though the biomass in these regions is much lower (Figure S13a). At the end of the century, there is a greater positive disequilibrium in most areas, and noticeably larger areas of positive disequilibrium in the gyres (Figure S13b). This general shift to more positive disequilibrium stems from a combination of declining ocean productivity and the system lags shown in Figure S11, especially for the low biomass / slow equilibriation gyre regions. Figures

S13c and S13d show the most "out of equilibrium" state variable of BORIS for the 1990s and the 2090s. Broadly, the global benthos is split between locations with excess seafloor detritus, i.e. more than at equilibrium, and those where the largest size class is most out of equilibrium. By the 2090s, the balance of this situation has shifted somewhat, such that the largest size class is most out of equilibrium over a larger portion of the world.

In general, intra- and inter-annual variations in seafloor POC flux introduce deviations, but as the three calibration sites illustrate, the dynamical simulation time-averages the equilibrium state quite closely (Figure S12b). Consequently, the future behaviour of BORIS can be accurately estimated using time-averaged seafloor POC fluxes and steady state calculations, at least for areas with non-negligible POC fluxes and shorter equilibriation times.

A key result from this study is a forecast decline in benthic biomass substantially greater than the corresponding decline in surface ocean productivity that drives it (see also Yool et al., 2013b). Jones et al. (2014) also examined the fate of benthic biomass in a multi-model study, finding a decline in productivity and near-seafloor POC flux (2000s $\rightarrow$ 2090s) of more than -11% that resulted in a decline in seafloor biomass of more than -5%. Our results appear more marked, so to make a direct comparison, we have forced the empirical model of Jones et al. (2014) with the same NEMO-MEDUSA output used in the present study (Appendix D). Table 4 indicates that when subject to common forcing regimes, the two models produce very similar outcomes. Comparing the broadly similar body size ranges of of total biomass in BORIS with macrofauna biomass in Jones et al. (2014), the respective changes are -6.2% and -7.3% under RCP 2.6 and -31% and -37% under RCP 8.5. These closely matched results derived from substantially different approaches point to the details of the POC flux forcing as being more important than the type of the benthic model being forced by that flux.

This study couples two models, each with their own limitations. Use of additional models of POC forcing could increase confidence in results, however, the performance of NEMO-MEDUSA has been extensively validated (Yool et al., 2013), and the present results suggest that the behaviour of BORIS is a relatively simple function of seafloor POC flux. Only monthly average POC flux forcing has been applied in the present case, and it is possible that shorter-term variability may operate in the field (Witte et al., 2003; Smith et al., 2014).

The BORIS model makes a number of assumptions and simplifications that influence its representation of the benthos and their ecology. As currently configured, BORIS omits organisms outside the reliable range of the calibration data. BORIS effectively represents seafloor microbes as "external" to the modelled system, i.e. they are ignored after they take a portion of the POC flux, and this overlooks the potential role of meio- and macrobenthos in preconditioning detrital substrates (Rowe and Deming, 2011). A practical consequence is the requirement for the f_{other} parameter, which makes specific assumptions and must be separately derived. It is possible to extrapolate the optimised model to both larger and smaller size classes (Ichino et al., 2015), but this was not done here in order to maintain model traceability with Kelly-Gerreyn et al. (2014).

BORIS also omits any consideration of the ecological roles played by temperature (Hunt and Roy, 2006), oxygen (Mosch et al., 2012) and ocean acidification (Andersson et al., 2011). For example, the Metabolic Theory of Ecology (Brown et al., 2004) would predict an inverse relationship between habitat temperature and standing stock biomass, with a

potential effect factor of 2 between extremes of present-day deep-sea temperatures. Similarly, recent work has highlighted the role of increasing temperature in reductions of body size (Reuman et al., 2014). These factors co-occur in climate change scenarios, with the potential for antagonistic effects, for instance, decreasing seafloor POC flux with enhanced habitat temperature (Mora et al., 2013). As Figure S14 illustrates, although NEMO-MEDUSA forecasts much of the deep seafloor to be only slightly affected by temperature change during the 21st century (mean change of 0.1°C), large temperature changes are predicted to occur in the most productive, shallow seas.

BORIS simplifies trophic relationships such that the modelled metazoans feed commensally from a common detrital pool. More generally, in representing organisms only by their body mass class, BORIS ignores mass-independent biological factors such as lifestyle (sessile, burrowing, swimming), feeding mechanism (deposit, filter, predation) and developmental mode (direct, lecithotrophic, planktotrophic), all of which may play a role in benthic system dynamics.

A significant limitation has been our use of globally uniform value of parameter f_{other}. Our calibration data suggest a value of 0.9 or more, but it remains unclear what the most appropriate value is. Consumption of incoming seafloor POC flux by microbes, and indeed the megabenthos, probably reflects both simple (e.g. POC quality) and complex factors (e.g. local community structure). We expect that f_{other} will vary systematically with the number of doubling body size classes that are explicitly modelled, in a manner comparable to the "energy equivalence rule" / "Damuth's rule" (White et al., 2007). Ideally, a "universal benthic model", grounded within the framework of allometry, should replace this parameter with a more explicit representation of the processes that it simplifies. A consistent way forward may be to extend the size range of organisms modelled to include microbes and megabenthos, and dispense with the f_{other} parameter.

BORIS (and other models; Wei et al., 2010) is formulated around the bulk flux of POC to the seafloor, and does not consider factors such as the type or quality of the material reaching benthic communities. Benthic metazoans of a broad size range certainly directly utilise energy from high quality carbohydrates in rapidly sedimenting phytodetritus (FitzGeorge-Balfour et al., 2010; Dunlop et al., 2016). However, the flux of material from the surface ocean will also include organic matter that has been extensively reworked in the surface and / or mesopelagic realms, which will be of much lower quality (Valls et al., 2014). In NEMO-MEDUSA, detritus is produced by a number of different processes acting on different model groups (phytoplankton, zooplankton), but BORIS only considers the first order seafloor POC flux. As such, it overlooks nutritional factors that may play a role in real systems, however knowledge of the significance of such aspects for benthic ecology is incomplete.

Despite these limitations, BORIS represents a dynamic, time-dependent alternative to empirical models such as Wei et al. (2010), and several avenues for future refinement are clear: extending the size range of organisms; including explicitly resolving microbes and their role in remineralisation; ecological relationships between metazoans and microbes (microbial gardening; Mayor et al., 2014) and between metazoans (predation).

A key driver of future work will be the assimilation of additional observational datasets, ideally from diverse sites that differ from those used in the initial development of BORIS. Our results on equilibriation times would suggest, in particular, examination of sites with very low seafloor POC fluxes to provide end members that can constrain model behaviour under

conditions of extreme oligotrophy. Additionally, similar time-lagged responses to climatic and upper ocean processes have been detected or inferred in abyssal benthic systems (Ruhl and Smith, 2004; Laguionie-Marchais et al., 2016). Incorporation of data from such sites will increase confidence when extrapolating to future situations in which local conditions have significantly departed from current. Such sites may also highlight environmental factors that are currently omitted from BORIS and which may drive its further development. Similarly, the assimilation of new seafloor POC flux datasets also represents a critical future avenue, especially where high temporal frequency sampling is achieved (Smith et al., 2014).

From a model-focused perspective, a potential extension to the work reported here would be to utilise BORIS in simulations forced with the output from a broader range of pelagic ecosystem models. For instance, from either the existing CMIP5 database (Jones et al., 2014), or those models participating in the upcoming CMIP6 exercise. As well as evaluating BORIS under a broader range of potential present-day and future conditions, exposure to different models may provide an impetus to consider factors beyond simple bulk POC flux, that some of these models, including NEMO-MEDUSA, can provide.

In summary, here we apply a body mass allometry-based model of benthic biomass, BORIS, to global scale and force it with time-varying seafloor POC fluxes from a model of pelagic biogeochemistry, NEMO-MEDUSA. We examined present-day patterns of seafloor biomass, and investigated how these may change into the future, using end-member climate change scenarios. For the present-day, forced by temporally-varying POC fluxes, BORIS exhibited strong seasonal and inter-annual behaviour, with distinct patterns of timing for different components under different forcings. Although there was considerable diversity in seasonal behaviour, mean annual benthic biomass was found to be strongly dependent on the seafloor POC flux, highlighting the importance of good quantification of this key flux. Compared with seasonality in seafloor POC flux, modelled seasonality in the seafloor detritus pool and benthic biomass was found to be much smaller, particularly with increasing individual body mass. These findings have potentially important implications both for which benthic components should be monitored, and for the frequency at which that monitoring should occur. Under future climate change scenarios, modelled benthic biomass was found to decrease to a greater degree than that of surface ocean productivity (-18% as compared to -6%), with deep-water communities experiencing greater declines than those in shallow seas. This is in accordance with patterns of seafloor POC fluxes in NEMO-MEDUSA, which are increasingly attenuated with water depth by future change, and with the dominant role of seafloor POC flux magnitude in BORIS. We note that absent forcing factors (temperature, oxygen, pH), and our simplified ecological assumptions (implicit microbes, trophic relations), represent important aspects for future development of BORIS, with the acquisition of observations from a broader range of seafloor environments of key importance.

Acknowledgements. The authors are grateful for the input and support provided by colleagues at the National Oceanography Centre in Southampton, in particular to B. Kelly-Gerreyn (now at the Australian Bureau of Meteorology). We would also like to thank the three anonymous referees and our editor, R. Kressman, for their comments and advice which greatly improved the manuscript.

The authors gratefully acknowledge the financial support of the Natural Environmental Research Council (NERC), UK, and the European Union Horizon 2020 programme. NERC support was provided by National Capability funding and the UK Earth System Model (UKESM) Long-Term Science Multi-centre programme. EU support was provided by the CRESCENDO project (grant number 641816).

Model output used in the production of this work is available from AY (axy@noc.ac.uk).

References

Andersson, A.J., Mackenzie, F.T. and Gattuso, J.-P.: Effects of ocean acidification on benthic processes, organisms, and ecosystems, in: Ocean Acidification, pp. 122–153, edited by: Gattuso, J., Hansson, L., Oxford University Press, Oxford, UK, 2011.

Behrenfeld, M.J. and Falkowski, P.G.: Photosynthetic rates derived from satellite-based chlorophyll concentration, Limnol. Oceanogr., 42, 1–20, 1997.

Bett, B.J.: Time-lapse photography in the deep sea, Underwater Tech., 25, 121–127, 2003.

Birchenough, S.N.R., Reiss, H., Degraer, S., Mieszkowska, N., Borja, A., Buhl-Mortensen, L., Braeckman, U., Craeymeersch, J., De Mesel, I., Kerckhof, F., Kroncke, I., Parra, S., Rabaut, M., Schroder, A., Van Colen, C., Van Hoey, G., Vincx, M., and Watjen, K.: Climate change and marine benthos: a review of existing research and future directions in the North Atlantic, WIREs Clim. Change 2015, 6, 203–223, doi: 10.1002/wcc.330, 2015.

Blanchard, J.L., Jennings, S., Law, R., Castle, M.D., McCloghrie, P., Rochet, M.-J., and Benoît, E.: How does abundance scale with body size in coupled size-structured food webs?, J. Anim. Ecol., 78, 270–280, 2009.

Blanchard, J.L., Heneghan, R.F., Everett, J.D., Trebilco, R., and Richardson, A.J.: From Bacteria to Whales: Using Functional Size Spectra to Model Marine Ecosystems, Trends in Ecology & Evolution, 32, 174–186, doi:10.1016/j.tree.2016.12.003, 2017.

Bopp, L., Resplandy, L., Orr, J.C., Doney, S.C., Dunne, J.P., Gehlen, M., Halloran, P., Heinze, C., Ilyina, T., Séférian, R., Tjiputra, J., and Vichi, M.: Multiple stressors of ocean ecosystems in the 21st century: projections with CMIP5 models, Biogeosciences, 10, 6225–6245, doi:10.5194/bg-10-6225-2013, 2013.

Brey, T., Müller-Wiegmann, C., Zittier, Z.M. C., and Hagen, W.: Body composition in aquatic organisms – A global data bank of relationships between mass, elemental composition and energy content, J. Sea Res., 64, 334–340, 2010.

Brey, T.: An empirical model for estimating aquatic invertebrate respiration, Methods Ecol. Evol., 1, 92–101, doi:10.1111/j.2041-210X.2009.00008.x, 2010b.

Brown, J.H., Gillooly, J.F., Allen, A.P., Savage, V.M., and West, G.B.: Toward a metabolic theory of ecology, Ecology, 85, 1771–1789, doi: 10.1111/1365-2656.12064, 2004.

Danovaro, R., Snelgrove, P.V.R., and Tyler, P.: Challenging the paradigms of deep-sea ecology, Trends in Ecology & Evolution, 29, 465–475, doi:10.1016/j.tree.2014.06.002, 2014.

Dickie, M., Kerr, S.R., and Boudreau, P.: Size-dependent processes underlying regularities in ecosystem structure, Ecol. Monogr., 57, 233–250, 1987.

Dunlop, K.M., van Oevelen, D., Ruhl, H.A., Huffard, C.L., Kuhnz, L.A. and Smith, K.L.: Carbon cycling in the deep eastern North Pacific benthic food web: Investigating the effect of organic carbon input, Limnol. Oceanogr., 61, 1956–1968, doi:10.1002/lno.10345, 2016.

Dunne, J.P., Sarmiento, J.L., and Gnanadesikan, A.: A synthesis of global particle export from the surface ocean and cycling through the ocean interior and on the seafloor, Global Biogeochem. Cy., 21, GB4006, doi:10.1029/2006GB002907, 2007.

FitzGeorge-Balfour, T., Billett, D.S.M., Wolff, G.A., Thompson, A., and Tyler, P.A.: Phytopigments as biomarkers of selectivity in abyssal holothurians; interspecific differences in response to a changing food supply, Deep Sea Res. Part II, 57, 1418–1428, doi: 10.1016/j.dsr2.2010.01.013, 2010.

Glazier, D. S.: Beyond the "3/4-power law": variation in the intra- and interspecific scaling of metabolic rate in animals, Biol. Rev. Camb. Philos., 80, 611–662, 2005.

Glazier, D.S.: A unifying explanation for diverse metabolic scaling in animals and plants, Biol. Rev., 85, 111–138, doi:10.1111/j.1469-185X.2009.00095.x, 2010.

Gooday, A.J., Bett, B.J., Shires, R. and Lambshead, P.J.D.: Deep-sea benthic foraminiferal species diversity in the NE Atlantic and NW Arabian sea: a synthesis, Deep-Sea Res. II, 45, 165–201, doi:10.1016/S0967-0645(97)00041-6, 1998.

Gruber, N.: Warming up, turning sour, losing breath: ocean biogeochemistry under global change, Phil. Trans. R. Soc. A, 369, 1980–1996, doi:10.1098/rsta.2011.0003, 2011.

Hain, M.P., Sigman, D.M. and Haug, G.H.: The Biological Pump in the Past, pp. 485–517, in: Treatise on Geochemistry, 2nd Edition, Elsevier, Amsterdam, Netherlands, doi:10.1016/B978-0-08-095975-7.00618-5, 2014.

Halfar, J. and Fujita, R.M.: Danger of Deep-Sea Mining, Science, 316, 987, doi: 10.1126/science.1138289, 2007.

Henson, S.A., Sanders, R. and Madsen, E.: Global patterns in efficiency of particulate organic carbon export and transfer to the deep ocean, Glob. Biogeochem. Cycles, 26, GB1028, doi:10.1029/2011GB004099, 2012.

Hildrew, A., Raffaelli, D., and Edmonds-Brown, R.: Body size: The structure and function of aquatic systems, Cambridge University Press, Cambridge, UK, 2007.

Honjo, S., Manganini, S.J., Krishfield, R.A., and Francois, R.: Particulate organic carbon fluxes to the ocean interior and factors controlling the biological pump: A synthesis of global sediment trap programs since 1983, Prog. Oceanogr., 76, 217–285, doi:10.1016/j.pocean.2007.11.003, 2008.

Hunt, G., and Roy, K.: Climate change, body size evolution, and Cope's Rule in deep-sea ostracodes, Proc. Nat. Acad. Sci., 103, 1347–1352, doi:10.1073/pnas.0510550103, 2006.

Huvenne, V.A.I., Bett, B.J., Masson, D.G., Le Bas, T.P., and Wheeler, A.J.: Effectiveness of a deep-sea cold-water coral Marine Protected Area, following eight years of fisheries closure, Biological Conservation, 200, 60–69, doi:10.1016/j.biocon.2016.05.030, 2016.

Ichino, M.C., Clark, M.R., Drazen, J.C., Jamison, A., Jones, D.O.B., Martin, A.P., Rowden, A.A., Shank, T.M., Yancey, P.H. and Ruhl, H.A.: The distribution of benthic biomass in hadal trenches: A modelling approach to investigate the effect of vertical and lateral organic matter transport to the seafloor, Deep-Sea Res. I, 100, 21–33, 2015.

Jackson, J.B.C., Kirby, M.X., Berger, W.H., Bjorndal, K.A., Botsford, L.W., Bourque, B.J., Bradbury, R.H., Cooke, R., Erlandson, J., Estes, J.A., Hughes, T.P., Kidwell, S., Lange, C.B., Lenihan, H.S., Pandolfi, J.M., Peterson, C.H., Steneck, R.S., Tegner, M.J., and Warner, R.R.: Historical Overfishing and the Recent Collapse of Coastal Ecosystems, Science, 293, 629–637, doi:10.1126/science.1059199, 2001.

Jeffreys, R.M., Burke, C., Jamieson, A.J., Narayanaswamy, B.E., Ruhl, H.A., Smith, K.L. Jr, and Witte, U.: Feeding Preferences of Abyssal Macrofauna Inferred from In Situ Pulse Chase Experiments, PLoS ONE 8, e80510, doi:10.1371/journal.pone.0080510, 2013.

Jones, C.D., Hughes, J.K., Bellouin, N., Hardiman, S.C., Jones, G.S., Knight, J., Liddicoat, S., O'Connor, F.M., Andres, R.J., Bell, C., Boo, K.-O., Bozzo, A., Butchart, N., Cadule, P., Corbin, K.D., Doutriaux-Boucher, M., Friedlingstein, P., Gornall, J., Gray, L., Halloran, P.R., Hurtt, G., Ingram, W.J., Lamarque, J.-F., Law, R.M., Meinshausen, M., Osprey, S., Palin, E.J., Parsons Chini, L., Raddatz, T., Sanderson, M.G., Sellar, A.A., Schurer, A., Valdes, P., Wood, N., Woodward, S., Yoshioka, M., and Zerroukat, M.: The HadGEM2-ES implementation of CMIP5 centennial simulations, Geosci. Model Dev., 4, 543–570, doi:10.5194/gmd-4-543-2011, 2011.

Jones, D.O.B., Yool, A., Wei, C.-L., Henson, S.A., Ruhl, H.A., Watson, R.A. and Gehlen, M.: Global reductions in seafloor biomass in response to climate change, Glob. Change Biol., 20, 1861–1872, doi: 10.1111/gcb.12480, 2014.

Kelly-Gerreyn, B.A., Martin, A.P., Bett, B.J., Anderson, T.R., Kaariainen, J.I., Main, C.E., Marcinko, C.J., and Yool, A.: Benthic biomass size spectra in shelf and deep-sea sediments, Biogeosciences, 11, 6401–6416, doi:10.5194/bg-11-6401-2014, 2014.

Kriest, I. and Oschlies, A.: Swept under the carpet: organic matter burial decreases global ocean biogeochemical model sensitivity to remineralization length scale, Biogeosciences, 10, 8401-8422, doi:10.5194/bg-10-8401-2013, 2013.

Kutti, T., Fosså, J.H., Bergstad, O.A.: Influence of structurally complex benthic habitats on fish distribution. Mar. Ecol. Prog. Ser., 520, 175-190, 2015.

Laguionie-Marchais, C., Paterson, G.L.J., Bett, B.J., Smith, K.L., and Ruhl, H.A.: Inter-annual species-level variations in an abyssal polychaete assemblage (Sta. M, NE Pacific, 4000 m), Prog. Oceanogr., 140, 43–53, 2016.

Levin, L.A. and Le Bris, N.: The deep ocean under climate change, Science, 350, 766–768, doi:10.1126/science.aad0126, 2015.

Lotze, H.K., Lenihan, H.S., Bourque, B.J., Bradbury, R.H., Cooke, R.G., Kay, M.C., Kidwell, S.M., Kirby, M.X., Peterson, C.H., and Jackson, J.B.C.: Depletion, Degradation, and Recovery Potential of Estuaries and Coastal Seas, Science, 312, 1806–1809, doi:10.1126/science.1128035, 2006.

Madec, G.: NEMO reference manual, ocean dynamic component: NEMO–OPA, Note du Pole de modélisation, Institut Pierre Simon Laplace, Technical Report 27, Note du pôle de modélisation, Institut Pierre Simmon Laplace, France, No. 27, ISSN No. 1288–1619, 2008.

Main, C.E., Ruhl, H.A., Jones, D.O.B., Yool, A., Thornton, B. and Mayor, D.J.: Hydrocarbon contamination affects deep-sea benthic oxygen uptake and microbial community composition, Deep Sea Research 100, 79–87, doi:10.1016/j.dsr.2014.12.008, 2015.

Martin, J.H., Knauer, G.A., Karl, D.M., and Broenkow, W.W.: VERTEX: carbon cycling in the northeastern Pacific, Deep-Sea Res. Pt.I, 34, 267–285, 1987.

Mawbey, E.M. and Lear, C.H.: Carbon cycle feedbacks during the Oligocene-Miocene transient glaciation, Geology, 41, 963–966, doi: 10.1130/G34422.1, 2013.

Mayor, D.J., Sanders, R., Giering, S.L.C., and Anderson, T.R.: Microbial gardening in the ocean's twilight zone: Detritivorous metazoans benefit from fragmenting, rather than ingesting, sinking detritus, BioEssays 36, 1132-1137, doi:10.1002/bies.201400100, 2014.

McClain, C.R., Allen, A.P., Tittensor, D.P., and Rex, M.A.: Energetics of life on the deep seafloor, Prof. Nat. Acad. Sci., 109, 15366-15371, doi: 10.1073/pnas.1208976109, 2012.

Moodley, L., Nigam, R., Ingole, B., Prakash Babu, C., Panchang, R., Nanajkar, M., Sivadas, S.,van Breugel, P., van Ijzerloo, L., Rutgers, R., Heip, C.H.R., Soetaert, K., and Middelburg, J.J.: Oxygen minimum seafloor ecological (mal) functioning, J. Exp. Mar. Biol. Ecol., 398, 91–100, doi: 10.1016/j.jembe.2010.12.015, 2011.

Mora, C., Wei, C.-L., Rollo, A., Amaro, T., Baco, A.R., Billett, D., Bopp, L., Chen, Q., Collier, M., Danovaro, R., Gooday, A.J., Grupe, B.M., Halloran, P.R., Ingels, J., Jones, D.O.B., Levin, L.A., Nakano, H., Norling, K., Ramireze-Llodra, E., Rex, M., Ruhl, H.A., Smith, C.R., Sweetman, A.K., Thurber, A.R., Tjiputra, J.F., Usseglio, P., Watling, L., Wu, T., and Yasuhara, M.: Biotic and Human Vulnerability to Projected Changes in Ocean Biogeochemistry over the 21st Century, PLoS Biol 11, e1001682, doi:10.1371/journal.pbio.1001682, 2013.

Morris, K.J., Bett, B.J., Durden, J.M., Benoist, N.M.A., Huvenne, V.A.I., Jones, D.O.B., Robert, K., Ichino, M., Wolff, G.A., and Ruhl, H.A.: Landscape-scale spatial heterogeneity in phytodetrital cover and megafauna biomass in the abyss links to modest topographic variation, Scientific Reports, 6, doi:34080.10.1038/srep34080, 2016.

Mosch, T., Sommer, S., Dengler, M., Noffke, A., Bohlen, L., Pfannkuche, O., Liebetrau, V., and Wallmann, K.: Factors influencing the distribution of epibenthic megafauna across the Peruvian oxygen minimum zone, Deep Sea Res. Pt. I, 68, 123–135, doi: 10.1016/j.dsr.2012.04.014, 2012.

Nomaki, H., Heinz, P., Nakatsuka, T., Shimanaga, M., and Kitazato, H.: Species-specific ingestion of organic carbon by deep-sea benthic foraminifera and meiobenthos: In situ tracer experiments, Limnol. Oceanogr., 50, 134–146, doi:10.4319/lo.2005.50.1.0134, 2005.

Peters, R.H.: The ecological implications of body size, Cambridge University Press, Cambridge, UK, 1983.

Pfannkuche, O. and Soltwedel, T.: Small benthic size classes along the N.W. European Continental Margin: spatial and temporal variability in activity and biomass, Prog. Oceanogr., 42, 189–207, doi:10.1016/S0079-6611(98)00034-2, 1998.

Popova, E., Yool, A., Byfield, V., Cochrane, K., Coward, A.C., Salim, S.S., Gasalla, M.A., Henson, S.A., Hobday, A.J., Pecl, G.T., Sauer, W.H., and Roberts, M.J.: From global to regional and back again: common climate stressors of marine ecosystems relevant for adaptation across five ocean warming hotspots, Glob. Change Biol., 22, 2038-2053, doi: 10.1111/gcb.13247, 2016.

Ramirez-Llodra, E., Tyler, P.A., Baker, M.C., Bergstad, O.A., Clark, M.R., Escobar, E., Levin, L.A., Menot, L., Rowden, A.A., Smith, C.R., and Van Dover, C.L.: Man and the Last Great Wilderness: Human Impact on the Deep Sea, PLoS ONE, 6, e22588, doi: 10.1371/journal.pone.0022588, 2011.

Rees, H.L., Boyd, S.E., Schratzberger, M., and Murray, L.A.: Role of benthic indicators in regulating human activities at sea, Env. Sci. Pol., 9, 496–508, doi: 10.1016/j.envsci.2006.04.002, 2006.

Reuman, D.C., Holt, R.D., and Yvon-Durocher, G.: A metabolic perspective on competition and body size reductions with warming, J. Anim. Ecol., 83, 59–69, doi: 10.1111/1365-2656.12064, 2014.

Rogelj, J., Meinshausen, M., and Knutti, R.: Global warming under old and new scenarios using IPCC climate sensitivity range estimates, Nature Climate Change, 2, 248–253, doi:10.1038/NCLIMATE1385, 2012.

Rowe, G.T. and Deming, J.W.: An alternative view of the role of heterotrophic microbes in the cycling of organic matter in deep-sea sediments, Mar. Biol. Res., 7, 629–636, doi:10.1080/17451000.2011.560269, 2011.

Ruhl, H.A., and Smith, K.L.: Shifts in deep-sea community structure linked to climate and food supply, Science 305, 513–515, 2004.

Schmidt-Nielsen, K.: Scaling – why is animal size so important?, Cambridge University Press, Cambridge, UK, 1984.

Schramski, J.R., Dell, A.I., Grady, J.M., Sibly, R.M., and Brown, J.H.: Metabolic theory predicts whole-ecosystem properties, Proc. Nat. Acad. Sci. 112, 2617–2622, doi:10.1073/pnas.1423502112, 2015.

Smith, K.L., Jr., and Kaufmann, R.S.: Long-Term Discrepancy Between Food Supply and Demand in the Deep Eastern North Pacific, Science, 284, 1174–1177, doi:10.1126/science.284.5417.1174, 1999.

Smith, K.L., Jr., Ruhl, H.A., Bett, B.J., Billett, D.S.M., Lampitt, R.S., and Kaufmann, R.S.: Climate, carbon cycling, and deep-ocean ecosystems, Proc. Nat. Acad. Sci., 106, 19211–19218, 10.1073/pnas.0908322106, 2009.

Smith, K.L., Jr., Sherman, A.D., Huffard, C.L., McGill, P.R., Henthorn, R., Von Thun, S., Ruhl, H.A., Kahru, M., and Ohman, M.D.: Large salp bloom export from the upper ocean and benthic community response in the abyssal northeast Pacific: Day to week resolution, Limnol. Oceanogr., 59, doi: 10.4319/lo.2014.59.3.0745, 2014.

Sweetman, A.K., Thurber, A.R., Smith, C.R., Levin, L.A., Mora, C., Wei, C.-L., Gooday, A.J., Jones, D.O.B., Rex, M., Yasuhara, M., Ingels, J., Ruhl, H.A., Frieder, C.A., Danovaro, R., Würzberg, L., Baco, A., Grupe, B., Pasulka, A., Meyer, K.S., Dunlop, K.M., Henry,

L.-A., Roberts, J.M.: Global climate change effects on deep seafloor ecosystems, Elementa: Science of the Anthropocene, 5:4, doi: 10.1525/elementa.203, 2017.

Valls, M., Sweeting, C.J., Olivar, M.P., de Puelles, M.L.F., Pasqual, C., Polunin, N.V.C., and Quetglas, A.: Structure and dynamics of food webs in the water column on shelf and slope grounds of the western Mediterranean, J. Mar. Syst., 138, 171–181, doi: 10.1016/j.jmarsys.2014.04.002, 2014.

Ward, B.A., Friedrichs, M.A.M., Anderson, T.R., and Oschlies, A.: Parameter optimisation techniques and the problem of underdetermination in marine bio-geochemical models, J. Marine Syst., 81, 34–43, 2010.

Wei, C.-L., Rowe, G.T., Escobar-Briones, E., Boetius, A., Soltwedel, T., Caley, M.J., Soliman, Y., Huettmann, F., Qu, F., Yu, Z., Pitcher, R., Haedrich, R.L., Wicksten, M.K., Rex, M.A., Baguley, J.G., Sharma, J., Danovaro, R., MacDonald, I.R., Nunnally, C.C., Deming, J.W., Montagna, P., Lévesque, M., Weslawski, J.M., Wlodarska-Kowalczuk, M., Ingole, B.S., Bett, B.J., Billett, D.S.M., Yool, A., Bluhm, B.A., Iken, K., Narayanaswamy, B.E.: Global patterns and predictions of seafloor biomass using random forests, PLoS ONE, 5, e15323, doi:10.1371/journal.pone.0015323, 2010.

White, E.P., Ernest, S.K.M., Kerkhoff, A.J., and Enquist B.J.: Relationships between body size and abundance in ecology, Trends Ecol. Evol., 22, 323–330, doi:10.1016/j.tree.2007.03.007, 2007.

Witte, U., Aberle, N., Sand, M. and Wenzhöfer, F.: Rapid response of a deep-sea benthic community to POM enrichment: an *in situ* experimental study, Mar. Ecol. Prog. Ser., 251, 27–36, 2003.

Yasuhara, M., Cronin, T.M., deMenocal, P.B., Okahashi, H., and Linsley, B.K.: Abrupt climate change and collapse of deep-sea ecosystems, Proc. Nat. Acad. Sci., 105, 1556–1560, doi:10.1073/pnas.0705486105, 2008.

Yasuhara, M., Okahashi, H., Cronin, T.M., Rasmussen, T.L. and Hunt, G.: Response of deep-sea biodiversity to abrupt deglacial and Holocene climate changes in the North Atlantic Ocean, Glob. Ecol. Biogeogr., 23, 957–967, doi:10.1111/geb.12178, 2014.

Yasuhara, M. and Danovaro, R.: Temperature impacts on deep-sea biodiversity, Biol. Rev., 91, 275–287, doi:10.1111/brv.12169, 2016.

Yool, A., Popova, E.E., and Anderson, T.R.: MEDUSA–2.0: an intermediate complexity biogeochemical model of the marine carbon cycle for climate change and ocean acidification studies, Geosci. Model Dev. Discuss., 6, 1259–1365, doi:10.5194/gmdd-6-1259-2013, 2013.

Yool, A., Popova, E.E., Coward, A.C., Bernie, D., and Anderson, T.R.: Climate change and ocean acidification impacts on lower trophic levels and the export of organic carbon to the deep ocean, Biogeosciences, 10, 5831–5854, doi:10.5194/bg-10-5831-2013, 2013b.

Yool, A., Popova, E.E., and Coward, A.C.: Future change in ocean productivity: Is the Arctic the new Atlantic?, J. Geophys. Res. Oceans, 120, 7771–7790, doi:10.1002/2015JC011167, 2015.

Additional Supporting Information may be found in the online version of this article:

Figure S1. Steady state biomass in the modelled size classes from individual site optimisations, and seasonal dynamics of seafloor detritus (R) and metazoan biomass (size classes 1–16).

Figure S2. Seasonal climatology of seafloor POC fluxes at the three geographical sites, and time-series (1980–2099) of mean annual seafloor POC fluxes at the three geographical sites.

Figure S3. Mean annual field of seafloor detritus.

Figure S4. Fields of the coefficient of variation (CoV) of key properties, and relationship between POC and seafloor detritus and biomass.

Figure S5. Average time lags between POC flux and seafloor detritus and total biomass.

Figure S6. Average time lags between POC flux and size class 1 and size class 16.

Figure S7. Average time lags between seafloor detritus maxima and size class 1 and size class 16.

Figure S8. Temporal and spatial distributions of seafloor biomass under scenario RCP 2.6.

Figure S9. Relationships between normalised changes (%) between the 1990s and the 2090s under RCP 8.5 for key properties.

Figure S10. Frequency distributions of relationships between coefficients of variation between the 1990s and the 2090s under RCP 8.5 for key properties.

Figure S11. The e-folding timescale of BORIS across the range of seafloor POC flux.

Figure S12. Time-series of total seafloor biomass at the three geographical sites for the dynamic simulation and analytical solution.

Figure S13. Relative disequilibrium and identity of most "out of equilibrium" component in the 1990s and 2090s.

Figure S14. Modelled seafloor temperature and 1990s to 2090s temperature change.

Table S1. Geometric body-mass size classes used in BORIS.

Table S2. Parameter values for BORIS based on optimisations at the FSC, FG and OM sites (Kelly-Gerreyn et al., 2014).

Table S3. Timing of seasonal maxima (days) of BORIS properties at the three sites.

Appendix A. Description, tuning, implementation, and analytical steady state solution of the BORIS model.

Appendix B. Description and forcing of the NEMO-MEDUSA model.

Appendix C. Additional description of results from the three geographical sites.

Appendix D. Description of the empirical benthic community model of Jones et al. (2014).

Table 1. Estimated and modelled seafloor POC fluxes (mg C m^{-2} d^{-1}) and corresponding f_{other} values. Row 1 lists the optimised POC fluxes (Q; Equation A4) consumed by modelled metazoans (Table S2). Row 2 lists the field POC fluxes to the seafloor (Table 1; Kelly-Gerreyn et al., 2014), together with the implied f_{other} values (–) required to produce the Q values above. The remaining rows list NEMO-MEDUSA output for the grid cells in which the geographical sites are located, and for the surrounding 3×3 cell neighbourhood. Averages for the period 1980–1999 from both the control and historical simulations are shown. In all NEMO-MEDUSA cases, the f_{other} values are those that would be required to produce the Q values at the top of the table.

Property	**POC flux**			**Estimated f_{other}**		
	FSC	**FG**	**OM**	**FSC**	**FG**	**OM**
Optimised Q	3.2	2.3	1.1	–	–	–
Observed POC flux	40	120	24	0.92	0.98	0.96
Control POC flux	4.8	100	3.7	0.34	0.98	0.70
3×3 cell region	4.8	85	4.2	0.34	0.97	0.74
History POC flux	4.2	91	4.5	0.25	0.98	0.75
3×3 cell region	4.5	77	4.8	0.29	0.97	0.77

Table 2. Average model forcing (primary and export production and seafloor POC flux), and average simulated seafloor biomass for the 1990s and 2090s under scenarios RCP 2.6 and RCP 8.5. Seafloor biomass is listed for seven water depth bands. For both scenarios, the percentage change between the 1990s and 2090s is indicated in brackets.

Property	**Units**	**1990s**	**2090s, RCP 2.6**		**2090s, RCP 8.5**	
Primary production	g C m^{-2} d^{-1}	0.314	0.318	(+1.4%)	0.295	(-6.1%)
Export production, 100m	g C m^{-2} d^{-1}	0.065	0.064	(-1.3%)	0.058	(-11.4%)
Seafloor POC flux	g C m^{-2} d^{-1}	0.029	0.032	(+8.4%)	0.028	(-3.9%)
Biomass, $\rightarrow$ 0.1 km	g wet wt m^{-2}	8.831	9.594	(+8.6%)	9.109	(+3.2%)
Biomass, $\rightarrow$ 0.2 km	g wet wt m^{-2}	7.603	7.735	(+1.7%)	7.545	(-0.8%)
Biomass, $\rightarrow$ 0.5 km	g wet wt m^{-2}	4.142	4.106	(-0.9%)	3.839	(-7.3%)
Biomass, $\rightarrow$ 1 km	g wet wt m^{-2}	1.887	1.806	(-4.3%)	1.551	(-17.8%)
Biomass, $\rightarrow$ 2 km	g wet wt m^{-2}	1.248	1.175	(-5.8%)	0.887	(-28.9%)
Biomass, $\rightarrow$ 5 km	g wet wt m^{-2}	1.067	0.992	(-7.0%)	0.725	(-32.0%)
Biomass, $\rightarrow$ 10 km	g wet wt m^{-2}	0.780	0.765	(-2.0%)	0.514	(-34.2%)
Globally-integrated biomass	Pg wet wt	0.607	0.600	(-1.1%)	0.500	(-17.6%)

Table 3. Seafloor area (10^6 km^2), POC flux to the seafloor (mg C m^{-2} d^{-1}) and modelled total biomass (g wet wt m^{-2}) listed at the global scale and for seven water depth bands for the 1990s and 2090s under scenarios RCP 2.6 and RCP 8.5. For both scenarios, the percentage change between the 1990s and 2090s is indicated in brackets.

Domain	**Area**	**POC flux**			**Total biomass**		
		1990s	**RCP 2.6**	**RCP 8.5**	**1990s**	**RCP 2.6**	**RCP 8.5**
Global	365.4	0.029	+8.4%	-3.9%	1.664	-1.1%	-17.6%
Seafloor → 0.1 km	18.7	0.340	+17.3%	+10.2%	8.831	+8.6%	+3.2%
Seafloor → 0.2 km	7.5	0.232	+1.9%	-1.0%	7.603	+1.7%	-0.8%
Seafloor → 0.5 km	9.5	0.074	-2.3%	-13.0%	4.142	-0.9%	-7.3%
Seafloor → 1 km	8.2	0.017	-8.7%	-29.3%	1.887	-4.3%	-17.8%
Seafloor → 2 km	15.2	0.008	-12.2%	-47.3%	1.248	-5.8%	-28.9%
Seafloor → 5 km	256.1	0.006	-12.5%	-53.4%	1.067	-7.0%	-32.0%
Seafloor → 10 km	50.2	0.003	-7.2%	-56.3%	0.780	-2.0%	-34.2%

Table 4. Direct comparison of the BORIS model and the Jones et al. (2014) empirical analysis when driven by common NEMO-MEDUSA POC flux, at the seabed in the former, and at 500 m above bottom (mab) in the latter (Martin et al., 1987). Predicted POC flux and corresponding benthic biomass for the 1990s and the 2090s under the RCP 2.6 and RCP 8.5 senarios detailed in the text. BORIS total biomass (summed mass of modelled size classes) is taken to be broadly equivalent to the macrofauna category of Jones et al. (2014).

Model	**Property**	**Units**	**1990s**	**2090s, RCP 2.6**		**2090s, RCP 8.5**	
BORIS	POC seafloor flux	g wet wt m^{-2} d^{-1}	0.021	0.019	(-11.5%)	0.010	(-50.7%)
	"Total biomass"	g wet wt m^{-2}	1.059	0.993	(-6.2%)	0.728	(-31.2%)
Jones et al. (2014)	POC flux at 500 mab	g wet wt m^{-2} d^{-1}	0.032	0.029	(-10.1%)	0.018	(-42.8%)
	Macrofauna	g wet wt m^{-2}	1.373	1.270	(-7.3%)	0.855	(-37.3%)

Figure 1. **(a)** Schematic diagram of the components and interactions in the BORIS model. "Implicit respiration" refers to respiration by microbes and other unmodelled benthic organisms. **(b)** Map of the locations of the three sites used to originally parameterise the model. The grid cells and water depths shown are those of the NEMO model used in this study.

Figure 2. NEMO-MEDUSA simulated seafloor POC flux, as **(a)** mean and **(b)** coefficient of variation (CoV; based on monthly means to illustrate seasonality).

Figure 3. **(a)** Mean annual field of total modelled seafloor biomass (Figure S3 shows the corresponding field of seafloor detritus). **(b)** The relationship between mean annual POC and mean annual seafloor detritus (R; black) and biomass (classes 1–16; colours). Note that POC flux is expressed as g wet wt m^{-2} d^{-1}, and that logarithmic scales are used throughout.

Figure 4. Temporal and spatial distributions of seafloor total biomass under scenario RCP 8.5. **(a)** Time-series of mean annual seafloor total biomass by water depth bands (note: all lines are normalised to their 1990s averages). **(b)** Changes in seafloor total biomass between the 1990s and 2090s (note: the colour scale is logarithmic). Figure S8 details results under scenario RCP 2.6.

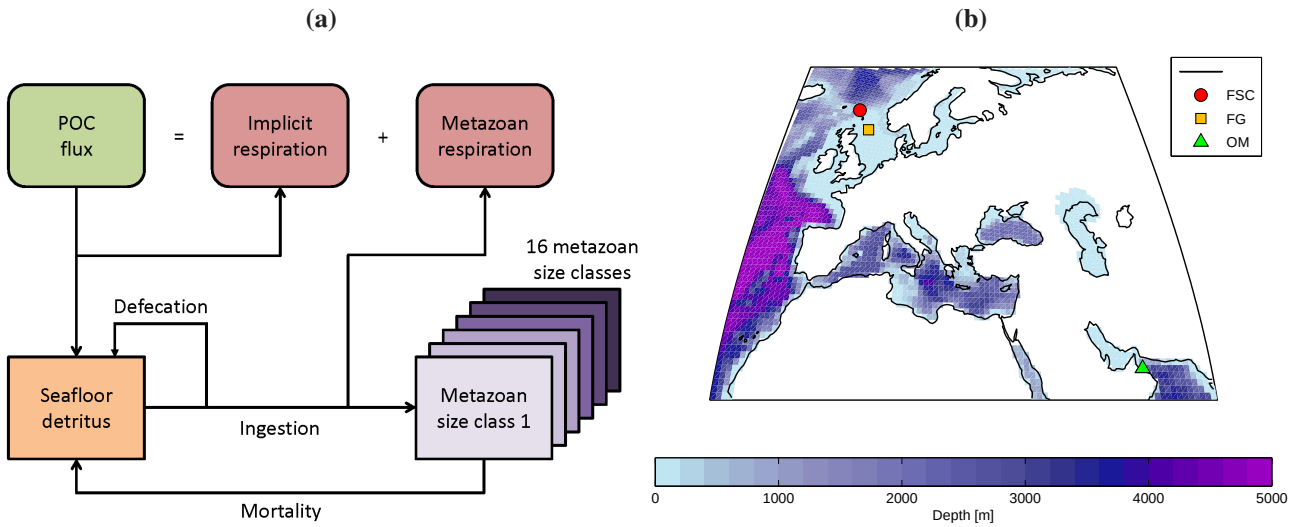

Figure 1. **(a)** Schematic diagram of the components and interactions in the BORIS model. "Implicit respiration" refers to respiration by microbes and other unmodelled benthic organisms. **(b)** Map of the locations of the three sites used to originally parameterise the model. The grid cells and water depths shown are those of the NEMO model used in this study.

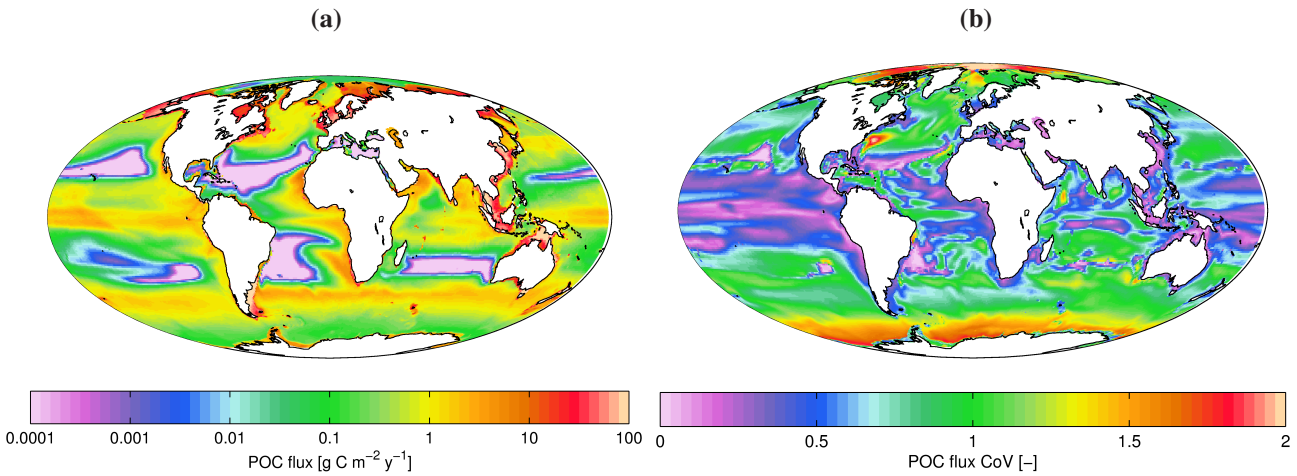

Figure 2. NEMO-MEDUSA simulated seafloor POC flux, as **(a)** mean and **(b)** coefficient of variation (CoV; based on monthly means to illustrate seasonality).

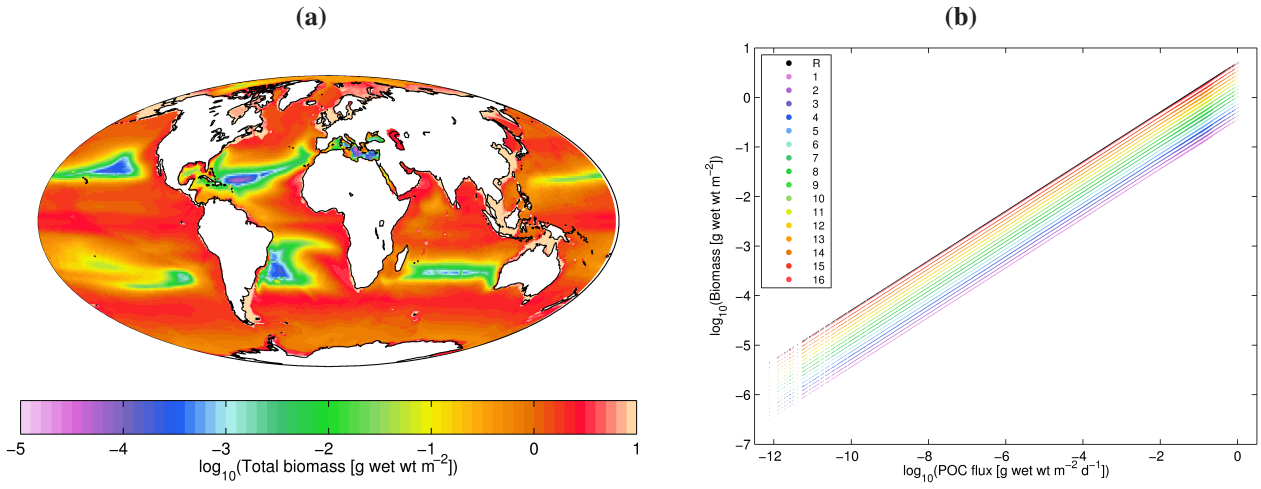

Figure 3. (a) Mean annual field of total modelled seafloor biomass (Figure S3 shows the corresponding field of seafloor detritus). **(b)** The relationship between mean annual POC and mean annual seafloor detritus (R; black) and biomass (classes 1–16; colours). Note that POC flux is expressed as g wet wt m^{-2} d^{-1}, and that logarithmic scales are used throughout.

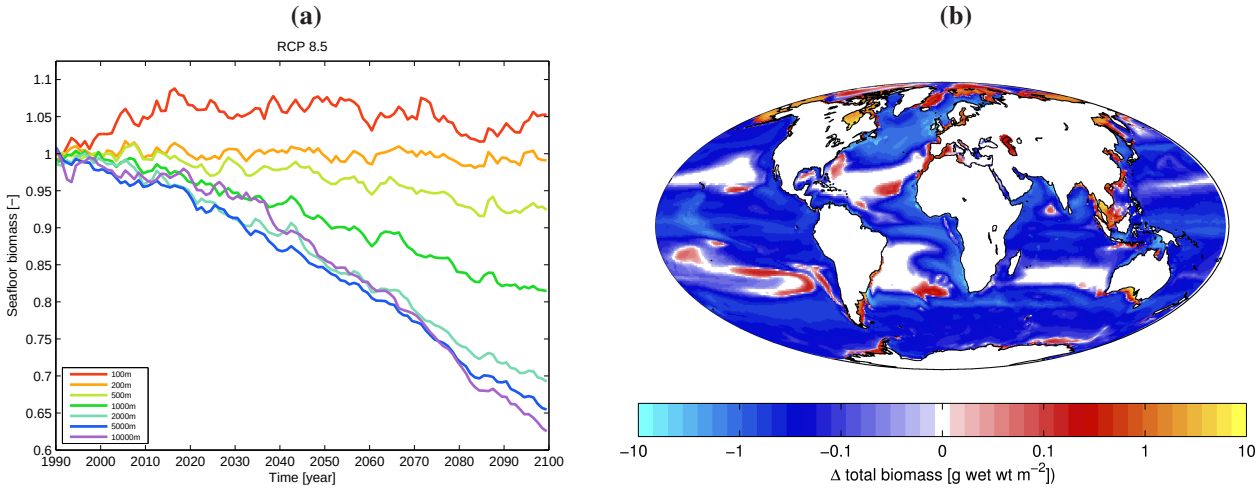

Figure 4. Temporal and spatial distributions of seafloor total biomass under scenario RCP 8.5. **(a)** Time-series of mean annual seafloor total biomass by water depth bands (note: all lines are normalised to their 1990s averages). **(b)** Changes in seafloor total biomass between the 1990s and 2090s (note: the colour scale is logarithmic). Figure S8 details results under scenario RCP 2.6.

Appendix A: BORIS

A1 Description

Based on field sampling, BORIS resolves 16 body mass classes of metazoans defined by a $\times 2$ geometric scale. These range from 8.9×10^{-7} to 2.8×10^{-2} g wet weight, and cover a spectrum of meio- and macro-benthos across a broad taxonomic range (Table S1). Inevitably, the model excludes organisms at both ends of this size spectrum, prokaryotes and small eukaryotes (e.g. bacteria, foraminiferans) at the small end, and megabenthos (e.g. the largest invertebrates, demersal fish) at the large end. Microbes may dominate the consumption of seafloor POC (Pfannkuche et al., 1999) and the model recognises this by including an implicit POC loss term that effectively delivers a residual proportion of the sinking POC flux to the modelled benthos. Omissions at the larger end are "rolled up" into this POC loss. Foraminiferans were specifically excluded from BORIS because of difficulties in reliably establishing the living protoplasmic mass of individuals.

The time-evolution of biomass for metazoans in BORIS, B_i, is calculated for each size class, i, by the following ordinary differential equation:

$$\frac{d\mathrm{B_i}}{dt} = \underbrace{\underbrace{+\underbrace{[\,\alpha \cdot I_i\,]}_{\text{assimilation}} - \underbrace{[\,r_i \cdot \alpha \cdot I_i\,]}_{\text{respiration}}}_{\text{net production}} - \underbrace{[\,m_i \cdot B_i^2\,]}_{\text{mortality}}} \tag{A1}$$

Where α is a constant assimilation efficiency for ingested detritus, r_i is the respiration coefficient for size class i expressed as a fraction of assimilation, m_i is a coefficient for mortality rate for size class i, and I_i is the ingestion rate for size class i. Ingestion is calculated here as:

$$I_i = g_i \cdot R \cdot B_i \tag{A2}$$

Where R is the stock of detrital material available as food, and g_i is an allometrically-varying ingestion coefficient. In all cases, the subscript i indicates that a property or parameter can be body-size dependent, and this ranges from 5–20.

Net production of metazoan biomass (i.e. growth) is calculated in equation A1 as the difference between the rates of assimilation and respiration. The loss terms are defecation (the fraction, $1-\alpha$, of ingestion not assimilated), mortality and respiration. The former two terms return POC to the detrital pool, while the latter term consumes POC, ultimately balancing the POC flux at steady state. Of these loss terms, note that defecation and respiration are functions of ingestion, while mortality is a function of the standing biomass of the different metazoan classes.

In Equations A1 and A2, first-order functions are used to model both ingestion and mortality, and the specific rates of these processes are regulated by the concentrations of detritus and biomass respectively. This use of density-dependent mortality (cf. Benoit and Rochet, 2004) prevents the competitive exclusion that would otherwise result with such a simple system where consumers share a common resource, and the stability of the resulting model was improved using a quadratic mortality term. Data to support this density-dependent formulation in the benthic realm are currently lacking, but this is a recognised mechanism for regulating populations in pelagic ecology (e.g. Ohman and Hirche, 2001; Minto et al., 2008).

Given the equations above, the time-evolution of the detrital pool available to the metazoan classes, is:

$$\begin{aligned} \frac{d\mathrm{R}}{dt} &= +\underbrace{[\,(1-f_{other})\,\cdot\,\mathrm{POC_{flux}}\,]}_{\mathrm{POC\,input}} \\ &\quad -\underbrace{\left[\sum_{i=5}^{i=20} I_i\right]}_{ingestion} + \underbrace{\left[\sum_{i=5}^{i=20} (1-\alpha)\,\cdot\,I_i\right]}_{defecation} \\ &\quad +\underbrace{\left[\sum_{i=5}^{i=20} m_i\,\cdot\,B_i^2\right]}_{mortality} \end{aligned} \tag{A3}$$

Where $\mathrm{POC_{flux}}$ is the flux of organic carbon sinking to the seafloor, and f_{other} is the fraction of this flux that is respired by unmodelled consumers (bacteria, foraminiferans, megabenthos). Note that, during tuning, these two parameters were instead conflated per Equation A4 into a single parameter, Q, because of the degeneracy of their relationship (i.e. tuned separately, multiple parameter solutions of low / high $\mathrm{POC_{flux}}$ / f_{other} would result). The other terms and parameters are those already described above, integrated here across the modelled metazoan size classes.

$$Q = (1-f_{other})\,\cdot\,\mathrm{POC_{flux}} \tag{A4}$$

As noted previously, metazoan size classes in BORIS are defined and parameterised using an allometric framework that scales key physiological rates with organism size. Three parameters, g_i, m_i and r_i are assumed to follow a power law that scales with body size such that:

$$\mathrm{PAR_i} = a\,\cdot\,W_i^b \tag{A5}$$

Where $\mathrm{PAR_i}$ is the value of the parameter for size class i, W_i is the size of organisms in class i, and prefactor a and scaling exponent b are estimated by fitting the model to observational data.

A more complete description of BORIS can be found in Kelly-Gerreyn et al. (2014).

A2 Tuning

The tuning process began with the specification of lower and upper values for each model parameter (per Table S2), and the division of the resulting range into a series of discrete and evenly-spaced intermediate values (64 in total). These discrete values of the 8 parameters become a "digital genotype" for a run that uses them (i.e. 8 parameters $\times$ 64 values = 8 $\times$ 2^6 = 48 binary digits).

Next, an ensemble of 8 individual "genotypes" was generated with randomly initialised parameter values (i.e. for each parameter, a random number between 1 and 64 was chosen, corresponding to one of the discrete values). These were simulated as the "first generation", then compared to observational data to generate a "cost" for each genotype.

The second generation was composed of the best (= lowest cost) genotype, plus 7 new genotypes formed by a process of random, but cost-weighted, combination of parameter values from the original 8 genotypes. This process of simulation, cost evaluation, selection of a "winner", and then creation of a successor generation was continued for 5000 generations at which point the lowest cost genotype was selected (fixation on a winning genotype typically occurred after around 2000 generations).

The whole procedure was then repeated 10 times for each geographical site, with the final "best" parameter set for each site being the lowest cost genotype from these 10 repeats. This repetition broadens the range of genotypes considered, and aims to circumvent the trapping of the genotypes within local minima of the cost function. Though omitted here for brevity, Kelly-Gerreyn et al. (2014) report the ranges of these 10 repeats.

In Ichino et al. (2015), and in the work here, a "unified" parameter set for BORIS is used. This was derived following the same basic optimisation procedure described above, but at each generation the 8 genotypes were simulated and evaluated at all three geographical sites simultaneously, with the resulting cost function reflecting unified performance. This modified process resulted in a single set of parameters which were able to represent all three geographical sites. Since the POC flux is known to vary geographically, the optimisation permitted site-specific POC fluxes (technically parameter Q) rather than a single fixed parameter.

Table S2 lists the resulting parameter sets for both individual geographical sites and the "unified" set.

A3 Implementation

As described in section A1, BORIS consists of a series of seventeen coupled ordinary differential equations, one for the seafloor detritus pool, R, and sixteen for the size-graduated biomass pools, B_i. These equations are coded up into the MATLAB package (R2013a) and integrated using the `ode15s` solver. The code is available upon request to `axy@noc.ac.uk`.

During the simulations described in the main text, BORIS is simulated at a single location driven by the time-varying POC forcing provided for that site by NEMO-MEDUSA. The global analysis presented in the main text is generated by combining the results from these individual "local" simulations into a spatially-resolved composite dataset.

By necessity simulations of BORIS are performed "offline", such that there is no feedback to NEMO-MEDUSA. In reality, remineralisation of organic material by the benthic community liberates nutrients which could drive further pelagic productivity, particularly in shallow water columns. Any long-term retention of nutrients by BORIS (or even burial; not currently included in the model) could represent a significant but much longer timescale feedback.

A4 Analytical steady state

For a time-constant POC_{flux}, the steady state biomasses of each size class, $\dot{B}_x$, and the seafloor detritus pool, $\dot{R}$, can be analytically determined as follows:

$$\dot{B}_x = \frac{\alpha \cdot (1-r_x) \cdot g_x \cdot \sqrt{Q} \cdot m_x^{-1}}{\sqrt{\sum_{i=5}^{i=20} \alpha^2 \cdot g_i^2 \cdot r_i \cdot (1-r_i) \cdot m_i^{-1}}} \quad \text{(A6)}$$

$$\dot{R} = \frac{m_x \cdot \dot{B}_x}{\alpha \cdot (1-r_x) \cdot g_x} \quad \text{(A7)}$$

Where the terms above correspond to those described in A1 and x is the metazoan size class index. In the case of equilibrium seafloor detritus, $\dot{R}$ can be calculated by substituting in any one of the 16 size classes of metazoan biomass.

In the work presented here, the steady state solution is used to provide initial conditions that are close to the model's dynamic equilibrium. This is necessary because the equilibriation time of BORIS increases dramatically with decreasing seafloor supply of POC. Figure S11 shows the e-folding timescale of equilibriation of BORIS across the range of POC fluxes produced by MEDUSA in simulations started with seafloor detritus pools that are double and half those calculated using the analytical steady state. Under the extremely low POC flux conditions that occur at abyssal depths in oligotrophic gyre regions, e-folding timescales can approach 1 My. Although these conditions are infrequent in MEDUSA, even perturbed ecosystems under higher POC flux conditions can take up to the cenntenial-scale to recover. Consequently, use of the analytical steady state to initialise simulations of BORIS removes the need for otherwise computationally expensive spin-up simulations.

Appendix B: NEMO-MEDUSA

B1 Description

The physical ocean component of NEMO-MEDUSA is the Nucleus for European Modelling of the Ocean (NEMO) model (Madec, 2008). This is composed of an ocean general circulation model, Océan PArallélisé version 9 (OPA9; Madec et al., 1998; Madec, 2008), coupled to a sea-ice model, Louvain-la-Neuve Ice Model version 2 (LIM2; Timmermann et al., 2005). OPA9 is a primitive equation model and is configured in this work at a "medium resolution" of approximately 1° horizontal resolution (362×292 grid cells) and 64 levels in the vertical. The horizontal grid is not uniform and features focusing of resolution around the equator to improve the representation of equatorial upwelling, as well as a tripolar configuration to avoid a grid singularity at the North Pole. In the vertical, levels increase in thickness with depth, from approximately 6 m at the surface to 250 m at 6000 m, with partial thickness cells at the seafloor to permit a more realistic representation of seafloor depth. The sea-ice submodel, LIM2, uses a viscous-plastic ice rheology (Hibler, 1979) with three layer (two $\times$ ice, one $\times$ snow) thermodynamics (Semtner, 1976; Timmermann et al., 2005). NEMO's sea-ice is coupled to its ocean every 5 ocean timesteps (Timmermann et al., 2005), and accounts for heat and freshwater fluxes driven by sea-ice formation/melting, precipitation and solar radiation penetration (Fichefet and Morales Maqueda, 1997; Timmermann et al., 2005).

The biogeochemical component is the Model of Ecosystem Dynamics, nutrient Utilisation, Sequestration and Acidification (MEDUSA-2; Yool et al., 2013). Though a simplified "intermediate complexity" model, MEDUSA-2 (henceforth MEDUSA) is designed to retain sufficient complexity to represent the primary feedbacks associated with climate change (CC) and ocean acidification (OA). It is founded on the nitrogen cycle and includes the elemental cycles of carbon (and alkalinity), silicon, iron and oxygen in a dual size-class nutrient-phytoplankton-zooplankton-detritus (NPZD) model. The modelled tracers include dissolved nitrogen, silicon and iron nutrients, "small" (nanophytoplankton and microzooplankton) and "large" (microphytoplankton and mesozooplankton) living components, as well as two pools of sinking detrital material. "Large" phytoplankton are assumed to be synonymous with diatoms in MEDUSA, and have a corresponding requirement for silicon (Mongin et al., 2006).

The POC flux to the seafloor is composed of two separate size classes of detrital particles. "Small" detritus is assumed to be slow-sinking and is modelled explicitly, while "large" detritus is assumed to be fast-sinking and is modelled implicitly using a variant of the Armstrong et al. (2002) ballast model (Klaas and Archer, 2002; Dunne et al., 2007). Here the ballast model is framed using biogenic fluxes of opal (Mongin et al., 2006) and calcium carbonate (Ridgwell et al., 2007). The balance of production, sinking and remineralisation means that, on average, shallow water regions are dominated by the flux of "small" detrital particles, while it is "large" particles that mostly reach the seafloor in deep water. Varied elemental ratios between the modelled groups, as well as processes such as differential remineralisation, mean that the C:N ratio of POM reaching the seafloor can be variable, but this work focuses solely on the POC component.

The implementation of the ballast model here implicitly remineralises POC down the water column each time-step, such that material produced in a single time-step is also remineralised during the same time-step. The assumption here is that the fast sinking velocity of "large" detrital particles both removes them rapidly from the euphotic zone where modelled zooplankton could consume them, and means that lateral transport by ocean currents is minimised. The use of such an implicit treatment of detrital sinking and remineralisation offers a reduced computational cost, since it effectively avoids the requirement to include 5 additional tracers. Note that slow-sinking, "small" detritus is modelled more conventionally as an explicit state variable with a sinking speed and a temperature-dependent remineralisation rate. As such, it has an extended lifespan, is a food source to model zooplankton, and may be transported horizontally (and vertically) by advection.

As part of a broad validation of the biogeochemical performance of NEMO-MEDUSA (including nutrients, carbon, productivity and ecological actors), Yool et al. (2013) includes a specific evaluation of the ocean interior POC fluxes that ultimately drive those at the seafloor. This comparison uses the synthesis database of Honjo et al. (2008), and compares the POC fluxes at a standardised depth of 2000 m. While this database is relatively small, and is biased towards deep ocean locations where POC fluxes are expected to be larger (i.e. away from unproductive – if large – oligotrophic areas), NEMO-MEDUSA agrees relatively well with it. Discrepancies in the performance of NEMO-MEDUSA, both positive and negative, are associated with mismatches in simulated productivity, in particular the Equatorial Pacific, where NEMO-MEDUSA is excessively productive, and at the margins of the oligotrophic regions, where it can be insufficiently productive.

POC that reaches the seafloor in MEDUSA falls into a "benthic bucket". This acts as a temporary reservoir from which POM is remineralised at a constant rate back to dissolved inorganic carbon and nutrients. It crudely represents the benthic community implicitly and serves to slow down the return of nitrogen, silicon and iron nutrients to bioavailable forms that can fuel pelagic productivity (note that carbon, being at high ambient concentration as DIC, is not generally believed to limit primary producers; but see Riebesell et al., 2007).

In MEDUSA, the POC flux to the seafloor is modelled in molar units of organic carbon, mol C m^{-2} d^{-1}. However, BORIS requires a POC flux in units of wet weight of organic material, g wet wt m^{-2} d^{-1}. To convert between these units, MEDUSA's POC flux is multiplied successively by the atomic mass of carbon (12.011), then by a factor converting carbon to dry weight (2.78), and finally by a factor converting dry weight to wet weight (4.55), following the relationships described by Brey et al. (2010).

More complete descriptions of NEMO-MEDUSA, including limited validation, can be found in Madec (2008; NEMO) and Yool et al. (2013; MEDUSA), and the model has previously participated in model intercomparison exercises (Popova et al., 2012; Kwiatkowski et al., 2014).

B2 Forcing

The simulations of NEMO-MEDUSA used here are forced at the ocean surface using output from simulations of the HadGEM2-ES Earth system model developed by the UK Meteorological Office (UKMO). This simulation was performed

as part of the UKMO's input to the Coupled Model Intercomparison Project 5 (CMIP5) (Jones et al., 2011) and Assessment Report 5 (AR5) of the Intergovernmental Panel on Climate Change (IPCC). The HadGEM2-ES simulations provided surface forcing fields of the same properties and frequencies as that of observationally-derived reanalysis datasets such as DFS4.1 (DRAKKAR Group, 2007) and CORE2 (Large and Yeager, 2009), namely 6-hourly for turbulent variables (air temperature, humidity and wind velocity), daily for radiation (downwelling short- and long-wave) and monthly for precipitation (rain, snow, runoff).

The historical simulation ran from start-1860 to end-2005 under historical atmospheric pCO_2 concentrations, and then branched for two parallel simulations from start-2006 to end-2099 under the IPCC Representative Concentration Pathways (RCP) 2.6 and 8.5 (i.e. up to 240 years duration in total). Both pathways are scenarios that include time series of climatically-active gases such as CO_2 and CH_4, and have been designed to produce specific radiative forcings by particular points in time. RCP 2.6 peaks at a radiative forcing of 3.0 W m^{-2} before 2100, while RCP 8.5 reaches greater than 8.5 W m^{-2} by 2100.

The control simulation uses a repeated 30-year cycle of forcing from the unperturbed portion of the historical simulation from start-1860 to end-1889. Atmospheric pCO_2 is kept at constant, pre-industrial concentrations throughout 8 cycles of this forcing (= 240 years; corresponding to a period of time of duration 1860–2099).

Further details about these simulations can be found in Yool et al. (2013; historical) and Yool et al. (2013b; future).

Appendix C: Site simulations

The following expands on Section 3.1 in the main body.

The relatively coarse grid of NEMO-MEDUSA means that direct site-to-cell mapping may create artificial discrepancies between inferred f_{other} values. To investigate this, we averaged across the nine cell (3 $\times$ 3) neighbourhood around each site, scaling to account for cell depth differences (i.e. where a neighbouring cell is shallower or deeper; this is particularly important at OM). While this does improve the inferred f_{other} values at both FSC and OM, the differences are relatively minor. The low value of f_{other} inferred at FSC (0.34) is consistent with a low productivity bias in the subpolar North Atlantic in NEMO-MEDUSA, noted by Yool et al. (2013) (though the lowest observationally-derived value of f_{other} is also from FSC). Focusing on FG and OM, the f_{other} values inferred using NEMO-MEDUSA in this way still range from around 0.74 to 0.98, a broader spread than those inferred from observations (0.92 to 0.98), but consistent with a minority fraction of the seafloor POC flux being available to the modelled metazoans.

The NEMO-MEDUSA values of seafloor POC flux reported in Table 1 are multi-decadal averages, but the model, as well as reality, exhibits temporal variability. To illustrate this, Figure S2 shows the seasonal cycle at each of the three sites averaged from the full 120 year control simulation, with the annual cycle represented by the median POC flux and its interannual variability by the interquartile range (note that single grid cells are used here and not the 3 $\times$ 3 neighbourhood). As already noted, the three sites differ markedly in the magnitudes of their seafloor POC fluxes, but they also differ strongly in the seasonal spread of these fluxes. At the FSC site, the POC flux is dominated by a peak in June, with near-zero flux during local winter. Meanwhile, at the FG site, the peak is both much higher and shifted slightly earlier to May, and local winter values, while lower, remain appreciable. Finally, at the OM site, the peak is earlier still, and the climatology exhibits an additional autumn peak in September. Interannual variability at all three sites is greatest around the seasonal maximum, and while otherwise reduced at the FSC and FG sites, remains modest throughout the year at the OM site.

On top of seasonal variability, NEMO-MEDUSA also exhibits marked interannual variability. To illustrate this, Figure S2 shows the time evolution of the POC flux at the three sites, integrated to annual averages. Alongside the control simulation, POC fluxes under RCPs 2.6 and 8.5 are also shown for comparison (see Section 3.3). While the FG site shows the largest absolute interannual variability, the relative variability is much greater at the two other sites, particularly the OM site. For reference, Figure S2 shows the corresponding POC fluxes from the 3 $\times$ 3 NEMO-MEDUSA cell neighbourhood at the site location.

Taking the seafloor POC fluxes shown in Figure S2 and applying them to BORIS at the three sites using a uniform value of f_{other} of 0.9, Figure S1b shows the resulting seasonal patterns of biomass for the modelled size classes as well as the seafloor detrital pool, R. Because of the spread of f_{other} values estimated in Table 1, we use a value of 0.9 inbetween those of sites FG and OM, and overlook that of FSC, where NEMO-MEDUSA is known to underpredict POC flux. The use of a single global value for f_{other} is discussed later. For each site, the plotted biomass is accompanied by a normalised indication of the seafloor

POC flux, as well as markers that note the timing of the seasonal maximum for the detritus and each size class. As Figure S1a has already shown, the quantity of biomass varies between the sites (FG $>$ FSC $>$ OM), and the quantity of biomass in each size class increases with size at all three sites.

More significantly, the panels show the temporal relationship between the POC flux to the seafloor, the detrital pool and the biomasses of the size spectrum of metazoans grazing on this. At all three sites, seafloor detritus generally reaches its annual maximum within a short period of the peak of seasonal POC flux. As Table S3 reports, the delay is shortest at FG (4 days), intermediate at FSC (25 days) and longest at OM (33 days). However, the timing of the biomass maxima, both in terms of individual size classes and for total biomass, can show much longer delays. At FSC, the seasonal biomass maximum occurs 90 days after peak detritus, with a range of 75–98 days from smallest to largest size classes. At FG, the delay is much reduced, 52 days for the biomass maximum and ranging 29–66 days. However, at OM, the delay is more than half a year, with 200 days for the biomass maximum and ranging 193–200 days up the size spectrum. These differences stem from a combination of model parameterisation and POC seasonality. The parameterisation of BORIS means that larger size classes respond more slowly than smaller ones, as is illustrated by Figure S1b's pattern of seasonal maxima.

Appendix D: Jones et al. (2014) model

Extending the empirical analysis of Wei et al. (2010), Jones et al. (2014) used a similar approach to that adopted here to explore the consequences for the benthos under different climate change scenarios. The model used in Jones et al. (2014) represents meiofaunal (sieve size 20–74 μm), macrofaunal (sieve size 250–520 μm) and megafaunal ($>$ 1 cm) benthos as empirical functions of the POC flux. The equations for these three groups are as follows:

$$\log_{10}(\text{meio}) = 1.4347 + (0.4428 \cdot \log_{10}(POC_{500\ m}) \quad \text{(D1)}$$

$$\log_{10}(\text{macro}) = 1.8422 + (0.6655 \cdot \log_{10}(POC_{500\ m}) \quad \text{(D2)}$$

$$\log_{10}(\text{mega}) = 1.4687 + (0.3948 \cdot \log_{10}(POC_{500\ m}) \quad \text{(D3)}$$

Where $POC_{500\ m}$ is the POC flux in mg C m^{-2} d^{-1} at 500 m above the local seafloor (regions shallower than 500 m are excluded from analysis). In Jones et al. (2014), $POC_{500\ m}$ is extrapolated from near-surface export production (both estimated and modelled) using the flux attenuation curve of Martin et al. (1987). The biomasses of the benthic components are in mg C m^{-2}.

Here, the model is forced using the same NEMO-MEDUSA seafloor POC fluxes as used with BORIS. For simplicity, these are amended to 500 m above the local seafloor by inverting the Martin et al. (1987) attenuation curve.

BORIS and Jones et al. (2014) represent the benthic community with different, non-overlapping size fractions of seafloor organisms. The most parsimonious comparison between the two models is that of total modelled biomass in BORIS and macrofaunal biomass in Jones et al. (2014).

References

Armstrong, R. A., Lee, C., Hedges, J. I., Honjo, S., and Wakeham, S. G.: A new, mechanistic model for organic carbon fluxes in the ocean: based on the quantitative association of POC with ballast minerals, Deep-Sea Res. II, 49, 219–236, 2002.

Benoit, E. and Rochet, M.-J.: A continuous model of biomass size spectra governed by predation and the effects of fishing on them, J. Theor. Biol., 226, 9–21, 2004.

DRAKKAR Group: Eddy-permitting Ocean Circulation Hindcasts of past decades, CLIVAR Exchanges, 42, 12, 8–10, 2007.

Fichefet, T., and Morales Maqueda, M.A.: Sensitivity of a global sea ice model to the treatment of ice thermodynamics and dynamics. J. Geophys. Res., 102, 12609–12646, 1997.

Hibler, W.D.: A dynamic thermodynamic sea ice model,J. Phys. Oceanogr., 9, 815–846, 1979.

Klaas, C. and Archer, D.: Association of sinking organic matter with various types of mineral ballast in the deep sea: implications for the rain ratio, Global Biogeochem. Cy., 16, 1116, doi:10.1029/2001GB001765, 2002.

Kwiatkowski, L., Yool, A., Allen, J.I., Anderson, T.R., Barciela, R., Buitenhuis, E.T., Butenschön, M., Enright, C., Halloran, P.R., Le Quéré, C., de Mora, L., Racault, M.-F., Sinha, B., Totterdell, I.J., and Cox, P.M.: iMarNet: an ocean biogeochemistry model inter-comparison project within a common physical ocean modelling framework, Biogeosciences Discuss., 11, 10537–10569, doi:10.5194/bgd-11-10537-2014, 2014.

Large, W.G. and Yeager, S.G.: The global climatology of an interannually varying air-sea flux data set, Climate Dynamics, 33, 341–364, doi:10.1007/s00382-008-0441-3, 2009.

Madec, G., Delecluse, P., Imbard, M., and Lévy, C.: OPA 8.1 Ocean General Circulation Model Reference Manual, Technical Report 11, Note du Pole de Modélisation, Institut Pierre Simon Laplace, Paris, France, 91 pp., 1998.

Minto, C., Myers, R.A., and Blanchard, W.: Survival variability and population density in fish populations, Nature, 452, 344–347, doi:10.1038/nature06605, 2008.

Mongin, M., Nelson, D.M., Pondaven, P., and Tréguer, P.: Simulation of upper–ocean biogeochemistry with a flexible–composition phytoplankton model: C, N and Si cycling and Fe limitation in the Southern Ocean, Deep–Sea Res. II, 53, 601–619, 2006.

Ohman, M.D. and Hirche, H.J.: Density-dependent mortality in an oceanic copepod population, Nature, 412, 638–641, doi:10.1038/35088068, 2001.

Pfannkuche, O., Boetius, A., Lochte, K., Lundgreen, U., and Thiel, H.: Responses of deep-sea benthos to sedimentation patterns in the north-east Atlantic in 1992, Deep-Sea Res. Pt. I,, 46, 573–596, 1999.

Popova, E.E., Yool, A., Coward, A.C., Dupont, F., Deal, C., Elliott, S., Hunke, E., Jin, M., Steele, M., and Zhang, J.: What controls primary production in the Arctic Ocean? Results from an intercomparison of five general circulation models with biogeochemistry, J. Geophys. Res., 117, 2156–2202, doi:10.1029/2011JC007112, 2012.

Ridgwell, A., Zondervan, I., Hargreaves, J.C., Bijma, J., and Lenton, T.M.: Assessing the potential long-term increase of oceanic fossil fuel CO_2 uptake due to CO_2-calcification feedback, Biogeosciences, 4, 481–492, doi:10.5194/bg-4-481-2007, 2007.

Riebesell, U., Schulz, K.G., Bellerby, R.G.J., Botros, M., Fritsche, P., Meyerhöfer, M., Neill, C., Nondal, G., Oschlies, A., Wohlers, J., and Zöllner, E.: Enhanced biological carbon consumption in a high CO_2 ocean, Nature, 450, 545–548, doi: 10.1038/nature06267, 2007.

Semtner, A.J.: A model for the thermodynamic growth of sea ice in numerical investigation of climate, J. Phys. Oceanogr., 6, 376–389, 1976.

Timmermann, R., Goosse, H., Madec, G., Fichefet, T., Ethe, C., and Duliere, V.: On the representation of high latitude processes in the ORCA-LIM global coupled sea ice-ocean model, Ocean Model., 8, 175–201, doi:10.1016/j.ocemod.2003.12.009, 2005.

Warwick, R.M.: Species size distributions in marine benthic communities, Oecologia, 61, 32–41, 1984.

Supplementary Tables

Table S1. Geometric body-mass size classes used in BORIS. These are adapted from the geometric size scale of Warwick (1984) in which each class is twice that in body-mass of the preceding class. The size sampling used in the observational studies that informed Kelly-Gerreyn et al. (2014) mean that the 16 size classes included in BORIS are numbered 5 through 20.

Size class (–)	Size class weight range (gram wet weight)			Geometric mean weight (gram wet weight)	Approximate wet weight (–)
5	6.0×10^{-7}	to	1.2×10^{-6}	8.4×10^{-7}	1 μg
6	1.2×10^{-6}	to	2.4×10^{-6}	1.7×10^{-6}	2 μg
7	2.4×10^{-6}	to	4.8×10^{-6}	3.4×10^{-6}	3 μg
8	4.8×10^{-6}	to	9.5×10^{-6}	6.7×10^{-6}	7 μg
9	9.5×10^{-6}	to	1.9×10^{-5}	1.3×10^{-5}	13 μg
10	1.9×10^{-5}	to	3.8×10^{-5}	2.7×10^{-5}	27 μg
11	3.8×10^{-5}	to	7.6×10^{-5}	5.4×10^{-5}	54 μg
12	7.6×10^{-5}	to	1.5×10^{-4}	1.1×10^{-4}	108 μg
13	1.5×10^{-4}	to	3.1×10^{-4}	2.2×10^{-4}	216 μg
14	3.1×10^{-4}	to	6.1×10^{-4}	4.3×10^{-4}	432 μg
15	6.1×10^{-4}	to	1.2×10^{-3}	8.6×10^{-4}	1 mg
16	1.2×10^{-3}	to	2.4×10^{-3}	1.7×10^{-3}	2 mg
17	2.4×10^{-3}	to	4.9×10^{-3}	3.5×10^{-3}	3 mg
18	4.9×10^{-3}	to	9.8×10^{-3}	6.9×10^{-3}	7 mg
19	9.8×10^{-3}	to	2.0×10^{-2}	1.4×10^{-2}	14 mg
20	2.0×10^{-2}	to	3.9×10^{-2}	2.8×10^{-2}	28 mg

Table S2. Parameter values for BORIS based on optimisations at the FSC, FG and OM sites (Kelly-Gerreyn et al., 2014), and optimised simultaneously for all three sites (All; Ichino et al., 2015). Parameter Q does not have a unified value but retains site-optimised values (see text for details). Note that for parameters g, m and r, the a components share the same units, while the b components are dimensionless (see Supplementary Equation A5).

Model parameter		**Allowed range**	**FSC**	**FG**	**OM**	**All**
Ingestion parameter, g	a_g	[0.1, 2.0]	1.8	0.6	1.5	1.76
(g wet weight)$^{-1}$ d^{-1}	b_g	[-0.5, 0.0]	-0.11	-0.18	-0.13	-0.13
Mortality parameter, m	a_m	[1.0×10^{-4}, 0.1]	7.2×10^{-4}	2.2×10^{-4}	2.4×10^{-3}	9.0×10^{-4}
(g wet weight)$^{-1}$ d^{-1}	b_m	[-0.5, 0.0]	-0.44	-0.43	-0.33	-0.4
Fraction of assimilation respired, r	a_r	[2.6×10^{-3}, 2.3]	0.58	0.88	0.38	0.61
–	b_r	[-0.39, 0.39]	8.4×10^{-3}	0.11	-0.87×10^{-3}	0.46×10^{-2}
Fraction of ingestion assimilated	α	[0.1, 0.9]	0.43	0.35	0.11	0.21
–						
POC flux available to metazoans	Q	[0.14, 275]	3.17	2.25	1.11	4.28, 5.64,
mg C m^{-2} d^{-1}						4.28

Table S3. Timing of seasonal maxima (days) of BORIS properties at the three sites under climatological control forcing (see text for details).

Property	FSC		FG		OM	
POC flux	167		137		77	
Seafloor detritus	192	+25	141	+4	110	+33
Smallest metazoan (1)	267	+100	172	+35	303	+226
Largest metazoan (16)	290	+123	207	+70	310	+233
Total metazoan biomass	282	+115	193	+56	310	+233

Supplementary Figures

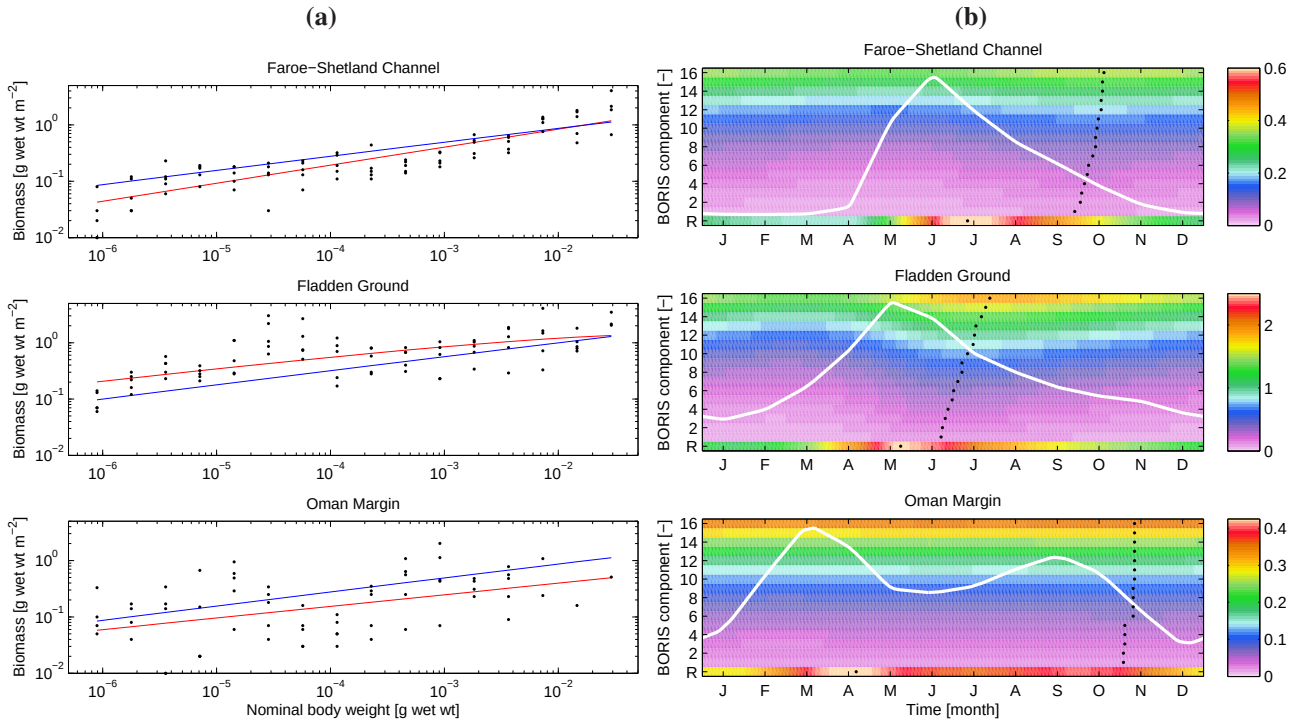

Figure S1. **(a)** Steady state biomass in the modelled size classes from individual site optimisations (red line; Kelly-Gerreyn et al., 2014) and the "unified" optimisations (blue line; this study), shown with field data (black dots). **(b)** Seasonal dynamics of seafloor detritus (R) and metazoan biomass (size classes 1–16), forced by climatological control POC flux. Colours represent biomass in each reservoir (black dots on indicate the annual maximum). The white line indicates normalised seafloor POC flux to illustrate the timing of forcing.

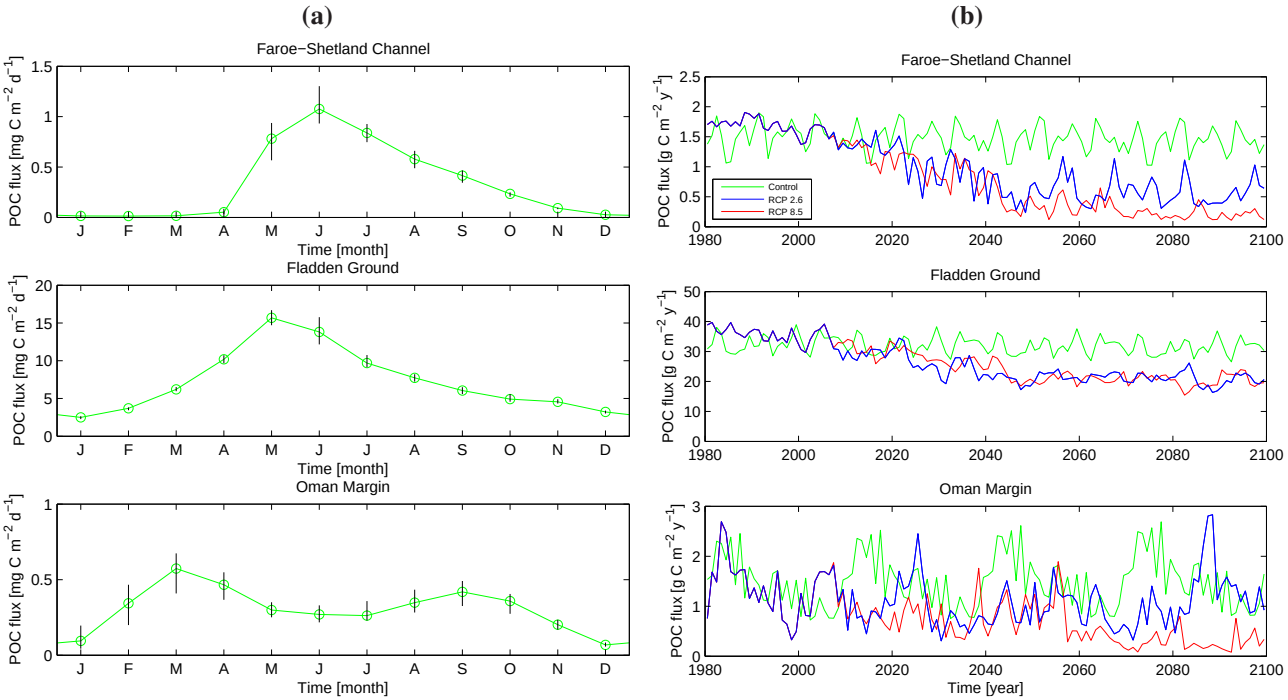

Figure S2. (a) Seasonal climatology of seafloor POC fluxes at the three geographical sites from the control simulation. The plot shows monthly medians (green circles and line) and interannual interquartile range (black lines). **(b)** Time-series (1980–2099) of mean annual seafloor POC fluxes at the three geographical sites from the control (green), RCP 2.6 (blue) and RCP 8.5 (red) simulations.

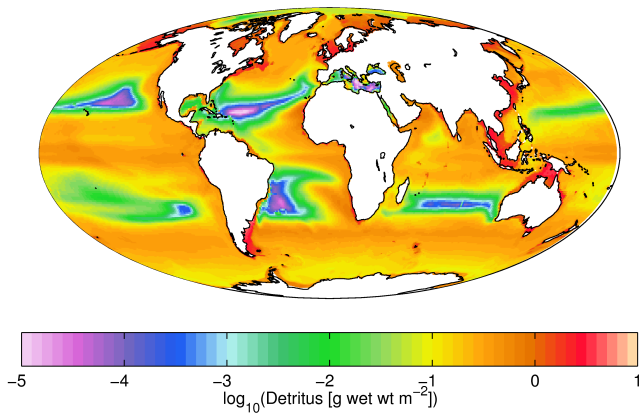

Figure S3. Mean annual field of seafloor detritus. Note that a logarithmic scale is used. Figure 3a shows the corresponding field of total seafloor biomass.

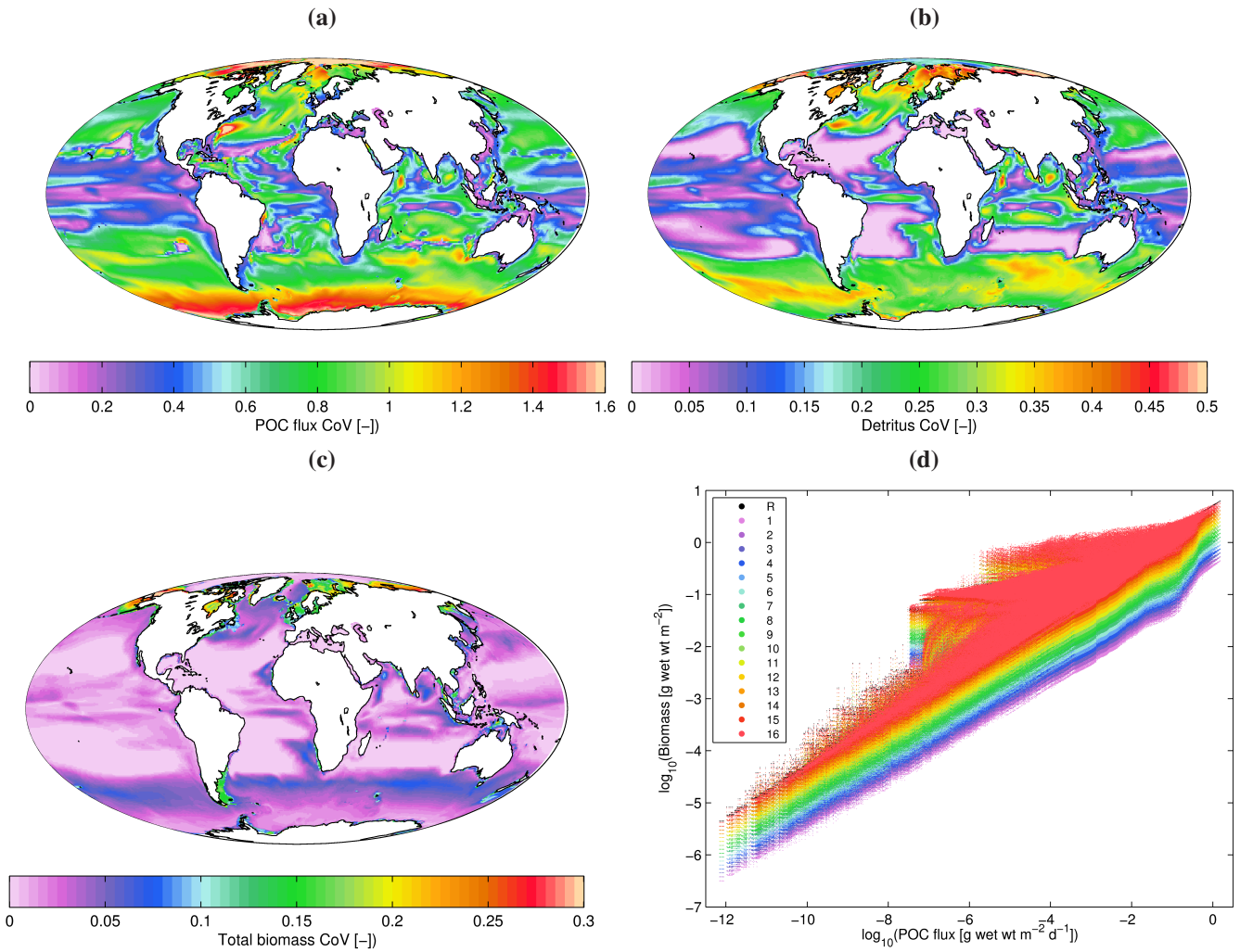

Figure S4. Fields of the coefficient of variation (CoV) of **(a)** POC flux, **(b)** seafloor detritus, and **(c)** total biomass. The relationship between mean monthly POC and mean monthly seafloor detritus and biomass is shown in **(d)** to illustrate the seasonal departure from the linear log–log relationship shown in Figure 3c.

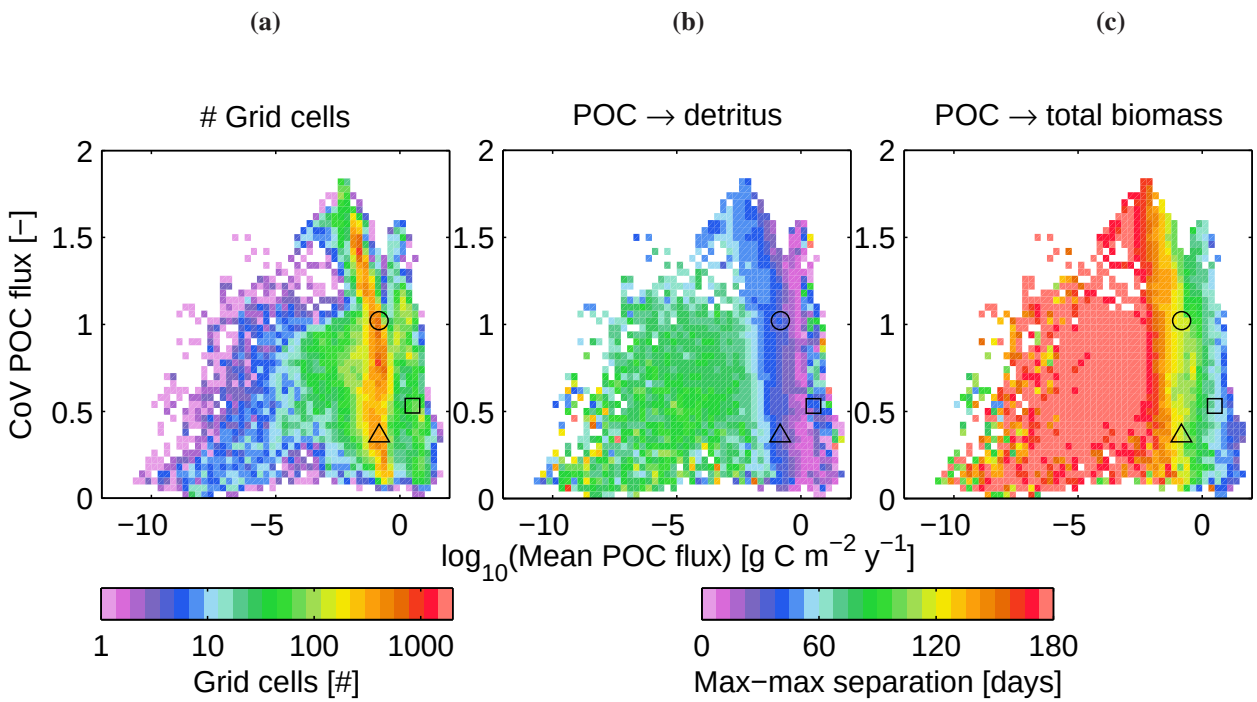

Figure S5. **(a)** Frequency distribution of NEMO-MEDUSA model grid cells by mean annual seafloor POC flux and corresponding CoV. Average time lag from annual maximum POC flux and annual maximum of: **(b)** seafloor detritus and **(c)** total biomass. The black symbols denote the FSC (circle), FG (square) and OM (triangle) calibration sites. Note that annual mean seafloor POC flux is shown in logarithmic bins.

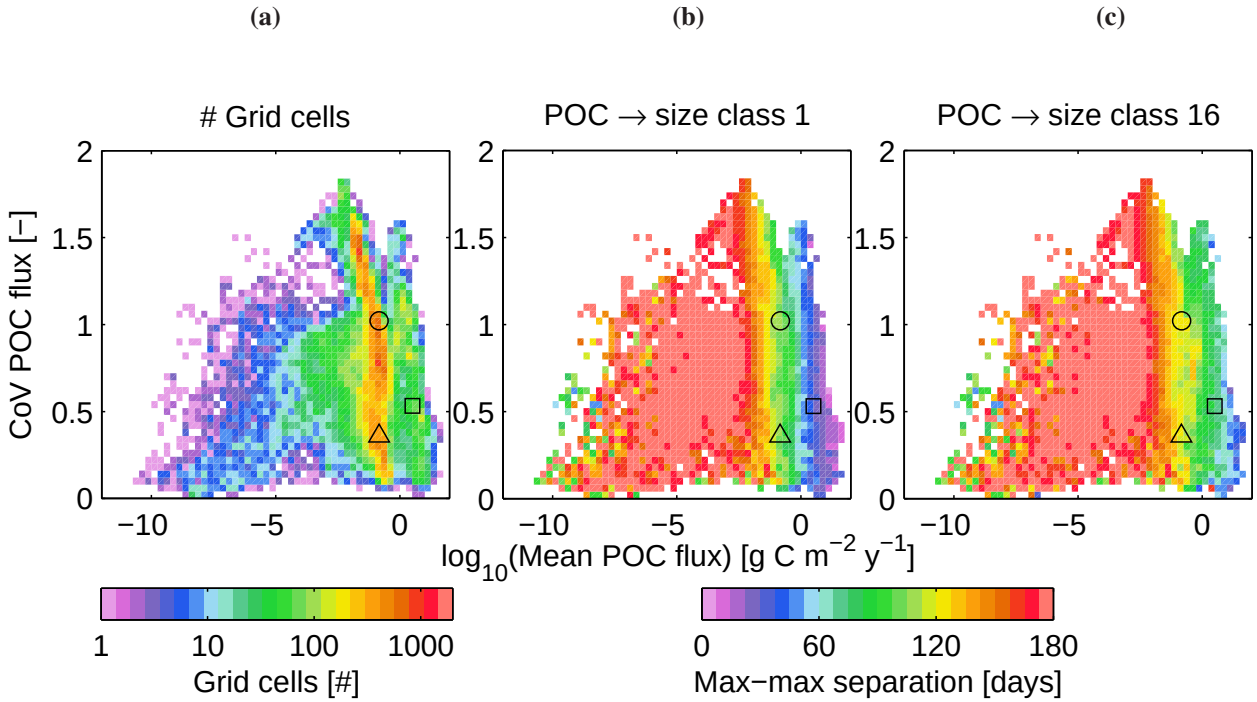

Figure S6. **(a)** Frequency distribution of POC flux by annual mean and CoV. The corresponding temporal gaps between annual maximum POC flux and annual maximum for **(b)** size class 1 and **(c)** size class 16. The black symbols denote where the FSC (circle), FG (square) and OM (triangle) sites occur in the illustrated space. Note that annual mean POC flux is shown on a logarithmic scale for clarity.

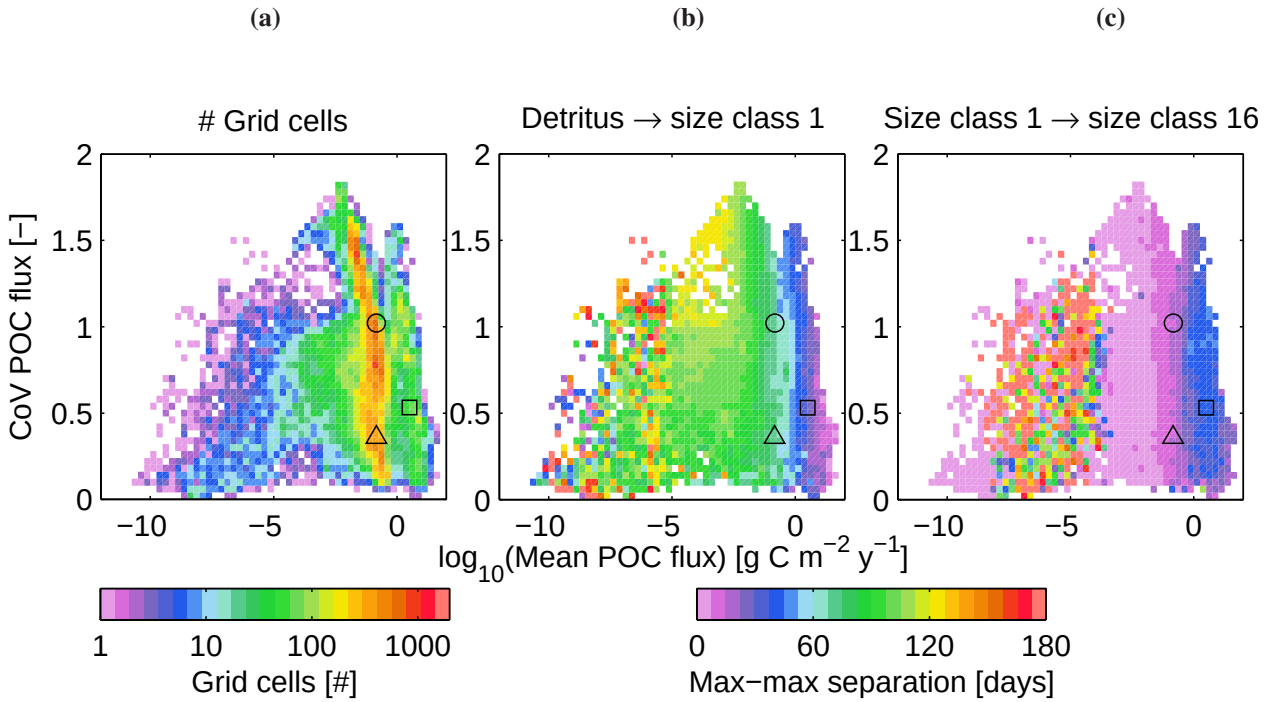

Figure S7. (a) Frequency distribution of POC flux by annual mean and CoV. The corresponding temporal gaps between **(b)** the annual maxima of detritus and size class 1, and **(c)** the annual maxima of size class 1 and size class 16. The black symbols denote where the FSC (circle), FG (square) and OM (triangle) sites occur in the illustrated space. Note that annual mean POC flux is shown on a logarithmic scale for clarity.

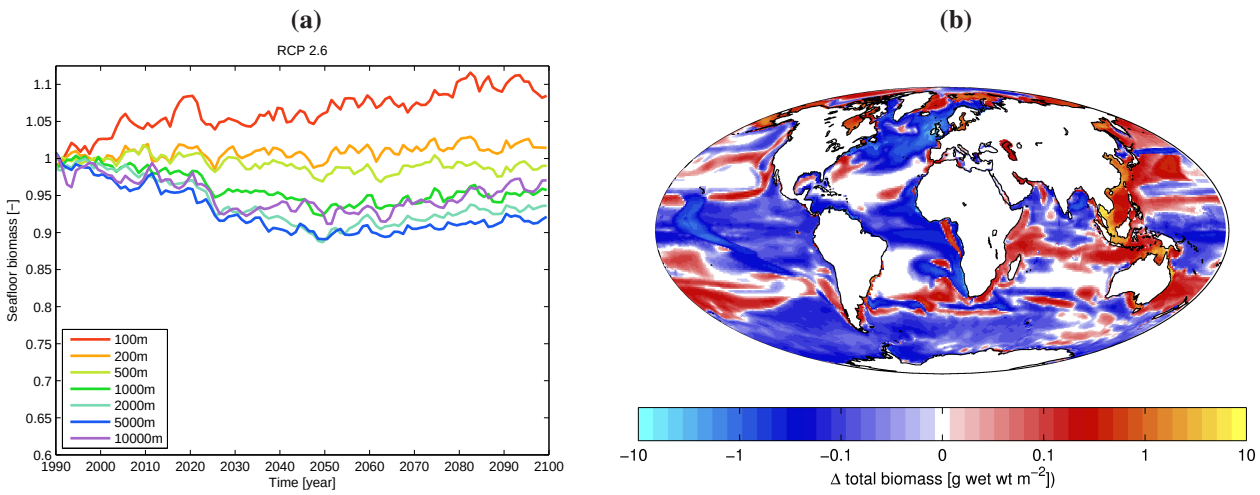

Figure S8. Temporal and spatial distributions of seafloor biomass under scenario RCP 2.6 **(a, b)**. Time-series of mean annual seafloor total biomass **(a)** for seafloor regions in different depth bands (per line colour). Because of the large span of values down the water column from high in the near-surface to low in the abyss, all lines are normalised to their 1990s averages. Changes in the geographical patterns of seafloor total biomass **(b)** between the 2090s and 1990s. Note that biomass change is not normalised, and that the colour scale uses logarithmic scaling. Figure 4 shows the corresponding results under scenario RCP 8.5.

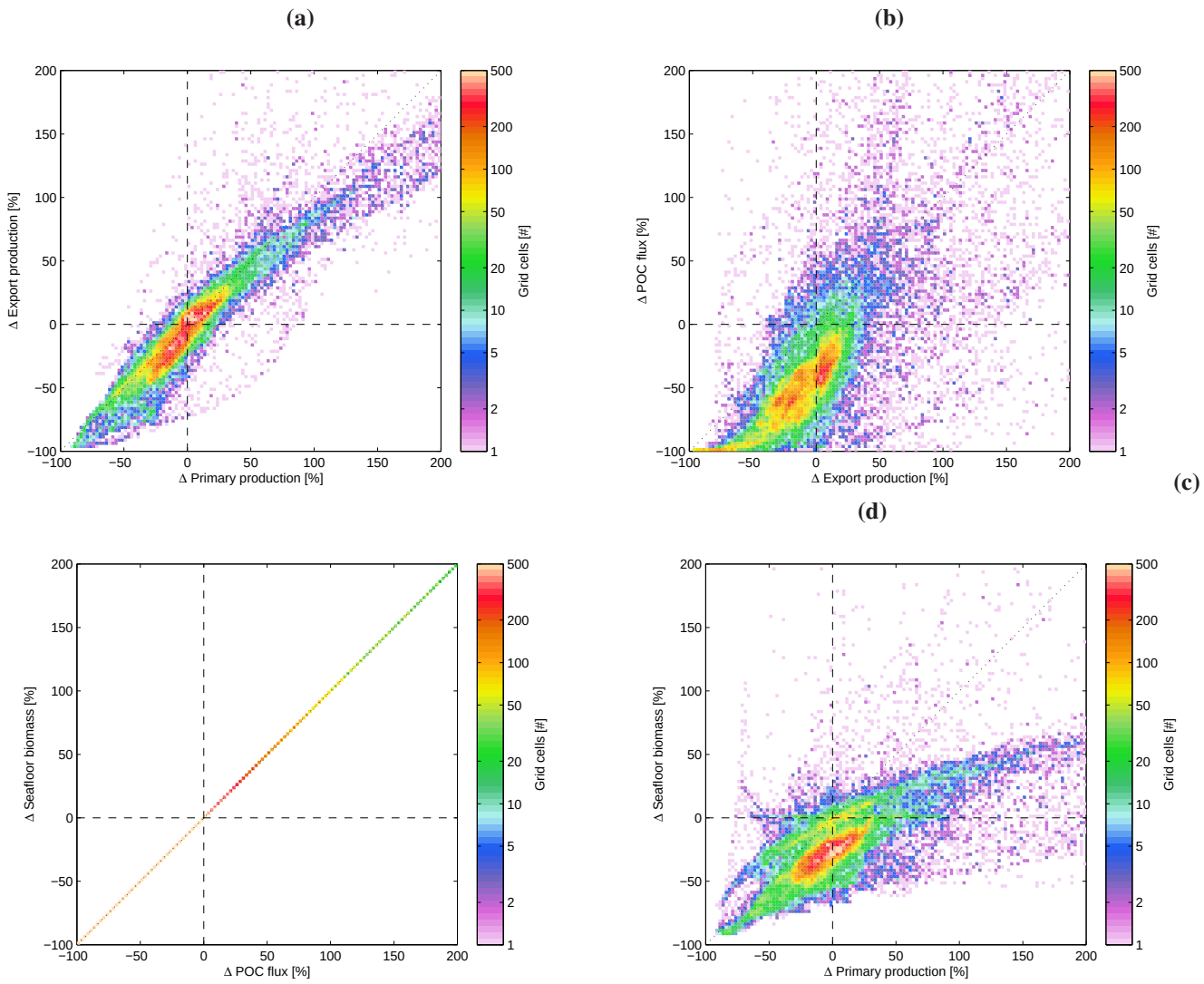

Figure S9. Relationships between normalised changes (%) between the 1990s and the 2090s under RCP 8.5 for **(a)** primary production and export production, **(b)** export production and seafloor POC flux, **(c)** seafloor POC flux and total modelled seafloor biomass, and **(d)** primary production and total modelled seafloor biomass. Dashed lines mark zero change in each property, and dotted lines denote the 1:1 relationship between properties.

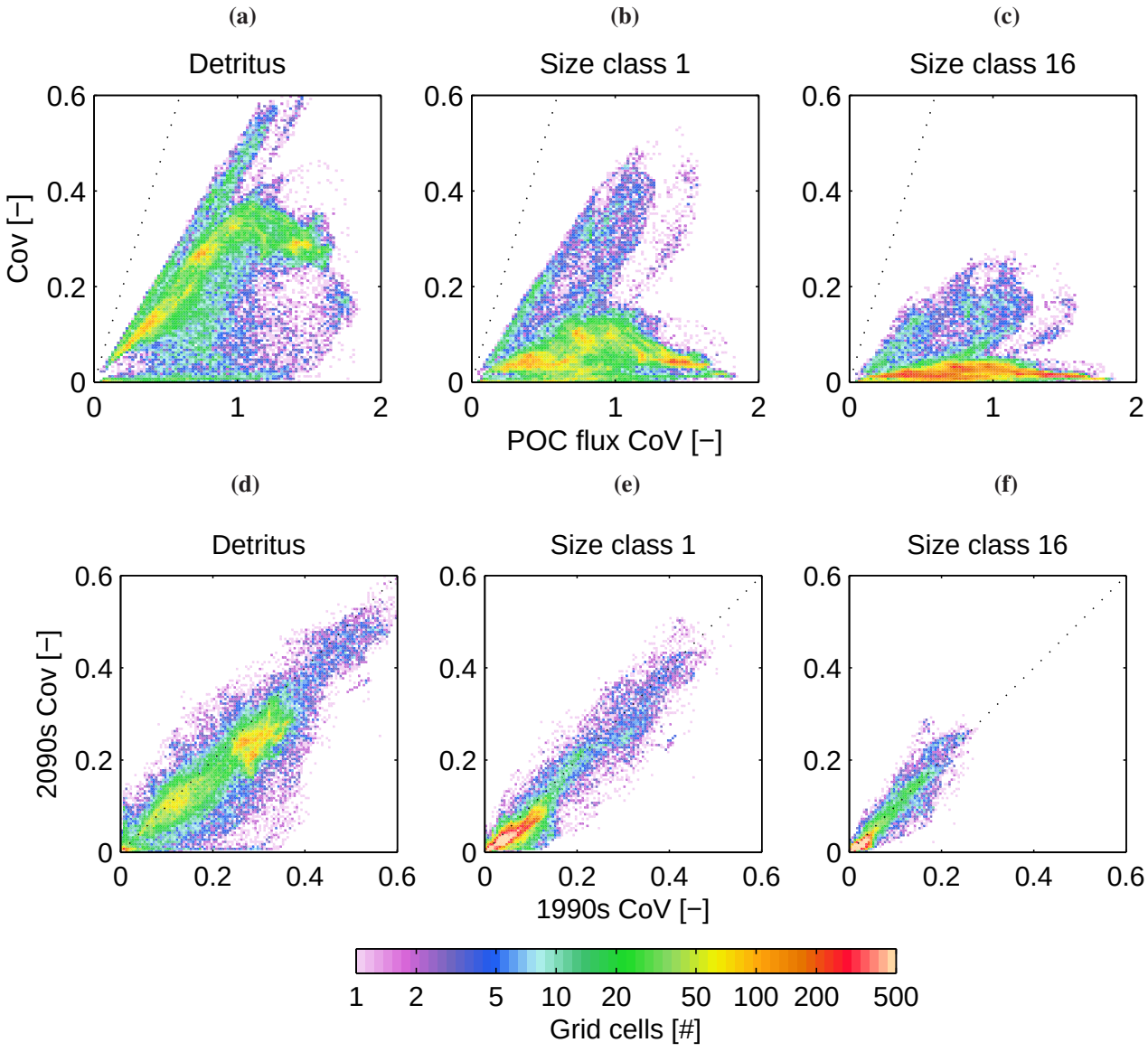

Figure S10. The upper row shows frequency distributions of seafloor POC flux CoV against **(a)** detritus CoV, **(b)** size class 1 CoV and **(c)** size class 16 CoV, in each case for the 1990s. The dotted lines indicate the 1:1 relationship, and illustrate the decline in CoV up the benthic food chain. The lower row shows frequency distributions of 1990s CoV against 2090s CoV for **(d)** detritus, **(e)** size class 1 and **(f)** size class 16. The dotted lines here again indicate the 1:1 relationship, and illustrate changes in the seasonality of these components across scenario RCP 8.5.

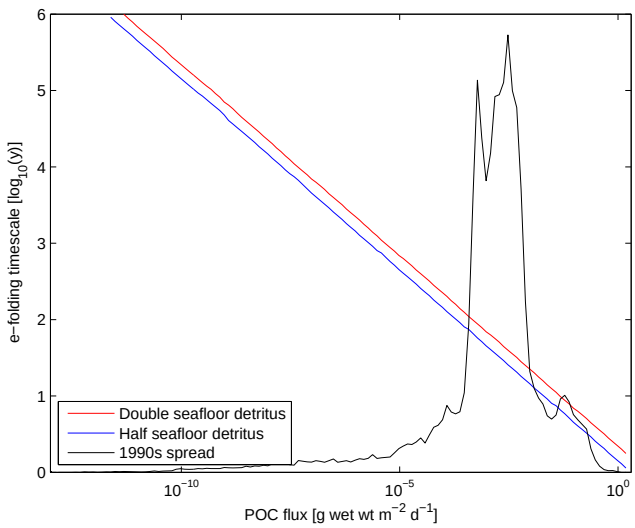

Figure S11. The e-folding timescale of BORIS across the range of seafloor POC flux simulated by MEDUSA. Equilibriation timescales are shown for simulations initialised with seafloor detritus pools that are double (red) and half (blue) those of the model's analytical steady state. Both x- and y-axes are shown on a log scale. The black line shows the corresponding frequency distribution of MEDUSA's seafloor POC fluxes for the 1990s. This y-axis of this line is linear, and the distribution is normalised for illustrative purposes.

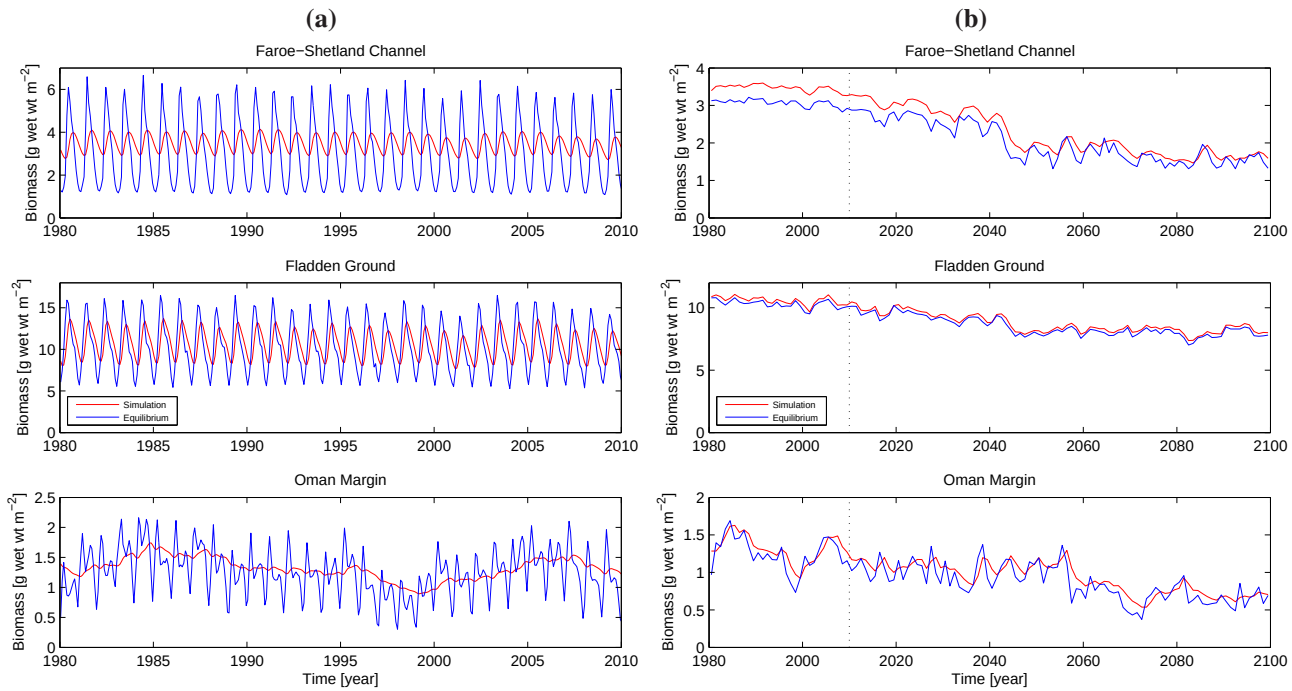

Figure S12. Time-series of total seafloor biomass at the three geographical sites averaged to **(a)** monthly (1990–2015) and **(b)** annual (1990–2099) frequencies. Results derived for the RCP 8.5 scenario for dynamic simulation (red) and analytical solution (blue) of BORIS. The dynamical simulation corresponds to results presented in the main body of the manuscript. The analytical solution is calculated (per Appendix A4) on the basis of monthly average POC fluxes, and then averaged to annual biomass for panel (b). The dotted lines in panel (b) mark the limit of the section shown in panel (a).

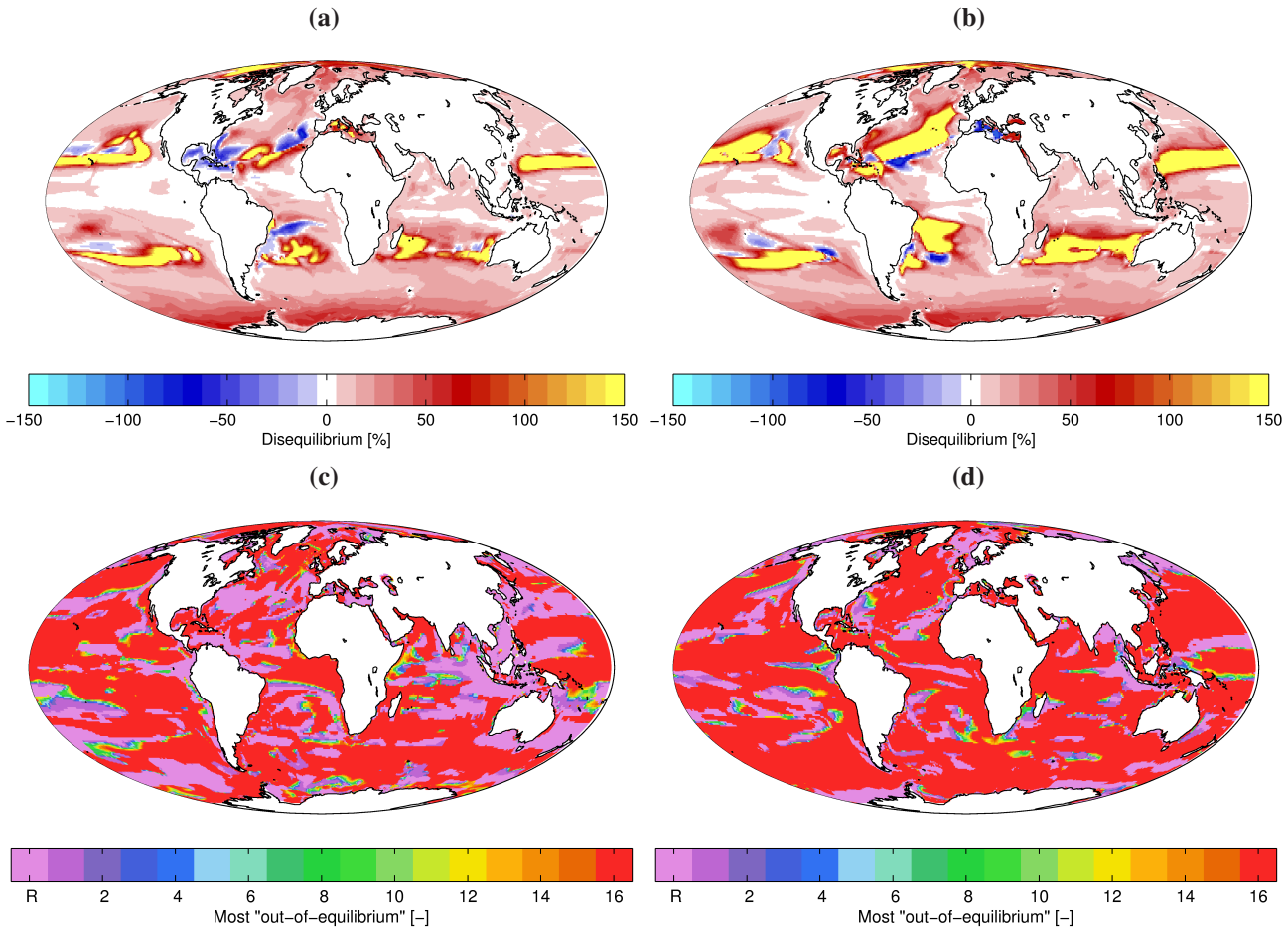

Figure S13. Relative disequilibrium of total seafloor biomass (in percent different from calculated equilibrium) for **(a)** the 1990s, and **(b)** the 2090s under RCP 8.5. Identity of the most "out of equilibrium" model component (largest relative difference with calculated equilibrium) for **(c)** the 1990s, and **(d)** the 2090s.

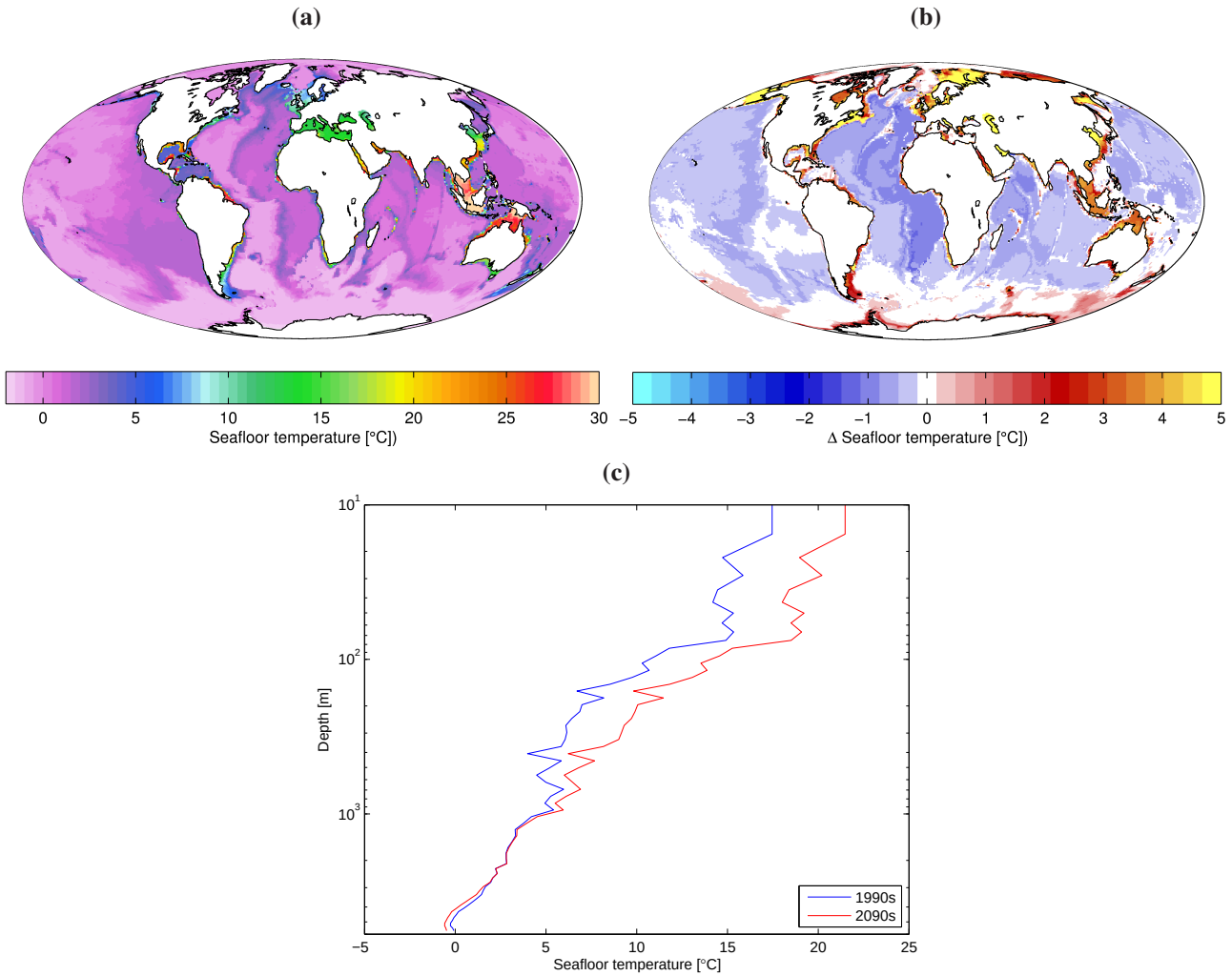

Figure S14. **(a)** Average seafloor temperature in NEMO for the 1990s. **(b)** Change in average seafloor temperature by the 2090s under RCP 8.5. **(c)** Depth profiles of average seafloor temperature for the 1990s and 2090s. Global average seafloor temperature change between these decades is 0.087°C.